MULTI-TEMPORAL CLASSIFICATION AND CHANGE DETECTION USING UAV IMAGES

SALMA A MAKUTI
February, 2018

SUPERVISORS:
Dr. F.C, Nex
Dr. M.Y, Yang

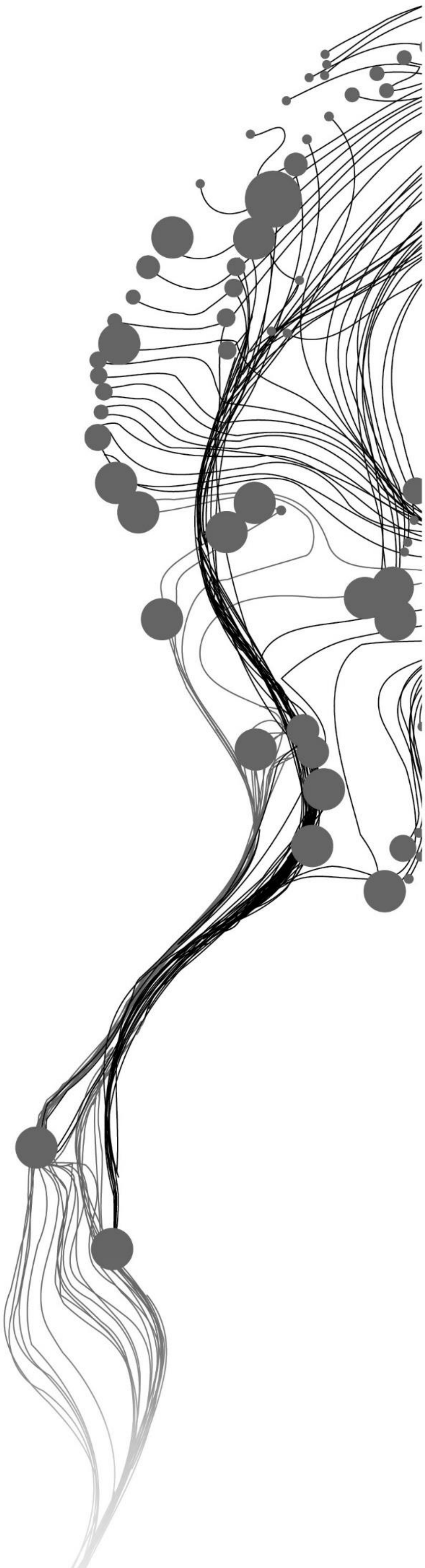

MULTI-TEMPORAL CLASSIFICATION AND CHANGE DETECTION USING UAV IMAGES

SALMA A MAKUTI
Enschede, The Netherlands, February, 2018

Thesis submitted to the Faculty of Geo-Information Science and Earth Observation of the University of Twente in partial fulfilment of the requirements for the degree of Master of Science in Geo-Information Science and Earth Observation.
Specialization: Geoinformatics

SUPERVISORS:
Dr. F.C, Nex
Dr. M.Y, Yang

THESIS ASSESSMENT BOARD:
Prof. Dr. Ir. M.G, Vosselman (Chair)
Dr. R.C, Lindenbergh (External Examiner, TU Delft)

ABSTRACT

Change detection is among the important image analysis techniques which help to understand how the area has been changing given a specific period. The importance of change detection includes monitoring and controlling land cover and land use changes, city planning and management and updating of the geographic information for a certain area. Change detection requires data to be repeatedly captured to have multi-temporal data. The introduction of UAV technology makes easier the capture of aerial and high resolution data. UAV is not only the cheapest platform for data acquisition, but it is also the easiest platform to operate and have control on the quality of data needed for a specific task.

In this thesis, we explore classification and change detection methods using orthophoto and DSM generated by UAV images. Three change detection methods have been evaluated including DSM change detection, post classification change detection technique and pre classification change detection technique. The data used in this thesis was taken in the construction area at Lausanne (Switzerland). A total of eight epochs was acquired from the beginning of the construction up to the end. Image differencing technique was used in DSM change detection followed by thresholding which was used to determine the change and unchanged area. Mathematical morphology operator opening was used to remove the noise in DSM change. By using orthophoto and DSM features as input, post classification and pre classification change detection was conducted to find the change in class between the epochs. For classification purposes, the conditional random field was used whereby unary potential was defined using random forest, and pairwise potential was defined using fully connected CRF. Experiment results show that post classification outperforms the pre classification change detection method. This was analysed using overall accuracy, whereby post classification have an accuracy of up to 63.9%, and the pre classification change detection has an accuracy of 46.5%.

Keywords: Change Detection, Random Forest, Fully Connected CRF, UAV images

ACKNOWLEDGEMENTS

I would first like to express my sincere thanks to the Almighty God for keeping me safe and with good health during my study time hear at the Netherlands, and for giving full protection of my family back home. I am very grateful forever.
I would also like to thank the Netherlands Fellowship Program (NFP) for believing in me and give me the opportunity for funding my study hear at University of Twente.
Special thanks go to my thesis supervisors, Dr. F.C, Nex and Dr. M.Y, Yang for the advice, comments, criticism and guidance in the right direction whenever they thought I needed help on how to conduct the research. This work could be nothing without your help and your patience.
To all GFM staffs, GFM students and student from other domains, I appreciate the company I had with you during my MSc studies. Special thanks go to my fellow students from Tanzania whom we spend most of the time together without forgetting our neighbours from Kenya I enjoy every good time I share with you all during my studies.
I want to express my sincere gratitude to my husband Ramadhan for the support and encouragement you have given me for the past 18 months of my study. You have always been there for my happiness and my sorrow, thank you for taking good care of our beloved sons it wasn't easy, but you have managed it.
To my mom Sharifa, I have nothing to pay you but God knows what you have been doing from the day you bring me to this world up to now, and you have never got tired God will reward you for that. Thank you for your prayers and for taking good care of my son. To my daddy Ahmad and my mother in law Mwajuma, may you continue to rest in eternal peace, I will always remember you for the love you have shown me and the support you have given me during your presence. To my siblings, Ahidnallah and Mpaji thank you very much for the love and support you have given me during my studies.

Salma A Makuti
Enschede, Netherlands
February 2018

TABLE OF CONTENTS

LIST OF FIGURES

LIST OF TABLES

APPENDICES

ABBREVIATIONS

UAV	–	Unmanned Aerial Vehicle
DSM	–	Digital Surface Model
CRF	–	Conditional Random Field
Veg	–	Vegetation
Bld	–	Building
Rd	–	Road
Bs	–	Bare soil
CNN	–	Convolutional Neural Network
OA	–	Overall accuracy
IoU	–	Intersect over Union

1. INTRODUCTION

1.1. Motivation and problem statement

The ever-increasing rate of urban growth in recent times has immensely transformed the urban landscapes world over. Urban sprawl leads to congestion of the immediate surroundings, as well as causing adverse effects including pollution and other processes that directly or indirectly cause Global Warming (Thomas Laidley, 2016). Due to this concern, Change Detection studies of urban systems has become an integral part for Urban and Regional Planning domains (Xu, Vosselman, & Oude Elberink, 2015). Change detection is one of the important image analysis research topics as it provides information about how the area has been changed at a specific time. The importance of change detection is mainly for monitoring and controlling the land cover and land use changes, city management and updating of the geographical information of a certain area (Liu et al., 2003).

Remote Sensing technologies have long been used for the analysis of change detection. Multi-temporal series of multi-spectral satellite imagery has played a major role in change detection studies for decades (Stow et al., 1990). Very high resolution (VHR) satellite images have shown to be a useful instrument in the monitoring of urban areas (Karantzalos, 2015) resulting in high accuracy in any image analysis compared to the traditional medium and low resolution satellite images (Bouziani et al., 2010). Despite the advantages of satellite images, there are some disadvantages. The disadvantages include not having direct control of the acquired image, having images which are affected by weather condition, by anyhow it is not possible to control the resolution of the acquired image as it is fixed already (Al Asmar, Koeva, & Gerke, 2017). However, the increase of new technology such as Unmanned Aerial Vehicle (UAV) has a big impact on the advancement of change detection due to its flexibility in the data acquisition. Most of the surveying task or airborne remote sensing activities can now be conducted much easily with UAV. It is easy to use UAV because it can be remotely controlled by the user and hence images can be acquired with different spatial and temporal resolution. But also camera used can be changed according to the application of the acquired image and high percentage overlap of up to 80% which reduce the risk of loss of information (i.e. occlusions in the scene).

In this regard, the use of UAVs for high resolution image acquisition has become a common platform in the geomatics field (Nex & Remondino, 2013), and proven to be good for urban area change detection up to the building level (Qin, 2014). When comparing to the past airborne sensors, UAV has got some advantages. These advantages includes the possibility of acquiring data in a small area at an affordable cost, does not require a highly skilled team for operation such as pilot which lower costs in the recruitment of staff as explained by Xuan (2011) though it requires a certified pilot in most of the countries.

Most of the monitoring activities require data to be repeatedly captured to have multi temporal data which can easily be implemented using UAVs. For the area where there is rapid development, constructions take place every day, UAVs could be of great help in updating the existing map of a considered area. UAV images can also be used for monitoring the progress of construction site after change detection analysis from the image acquired by it. They can also be used for damage mapping, topographic/cadastral mapping and cultural heritage documentation.

However, UAV images cannot be used directly for change detection because the raw data are the bunch of overlapping images. The acquired images need to be aligned in a photogrammetric workflow to generate Digital Surface Model (DSM) and orthophoto images using the co-registration presented in Aicardi et al. (2016). The generated orthophoto and DSM are the one that are used for further image analysis processes. In general, high resolution images from UAV can be very useful for the analysis of land cover, land use, as well as object extraction due to the high amount of information contained on them (Dalla Mura et al., 2009).

However, this can be a problem in classification processes due to the high amount of thematic information present in the images.

Most of the studies conducted for change detection analysis uses satellite images as their source of data (Argialas, Michailidou, & Tzotsos, 2013; Cao, Zhou, & Li, 2016; Yousif & Ban, 2017). Only a few have been done using UAV images (Qin, 2014; Unger, Reich, & Heipke, 2014). Unfortunately, the results from most of these works still suffer from noise problem, and they manage to detect only changed and unchanged area without classifying the changes.

Therefore, this study aims to accomplish automatic classification and change detection using DSM and orthophoto from different epochs as the product of UAV images. Three algorithms for change detection was used in this research. The first algorithm was used DSM as input to perform change detection, and the result was binary change (i.e. change and no change classes). The second and the third algorithm used orthophoto together with DSM features as input, and the results was the classified changes. A total of four classes was defined which are vegetation, building (concrete, roof), bare soil, road (road and railway). Some features like road and railway, concrete and roofs have to be combined due to the similarity of their spectral properties (Peiman, 2011).

In the second algorithm change between classes was extracted by overlaying two classified images of different epochs. This algorithm adopt conditional random field (CRF) model which has the ability to smoothen the boundaries of the classification results (Li & Yang, 2016) as well as removing false positive classified pixels. In the third algorithm change between the features was first generated followed by classification of those changes. Orthophoto and DSM features was used for change detection. Like the second algorithm, CRF model was also used for classification of changes. CRF model consist of unary potential and pairwise potential, whereby unary potential was defined by the selected classifier and the pairwise potential makes use of the contextual information on smoothening the results from the selected classifier. Some of the datasets was used for training and others used for testing the classifier, and the performance was evaluated using the accuracy assessment.

The dataset used in this research was collected using UAV platform, they are of very high resolution (5 cm Ground Sampling Distance) and have been acquired in 8 different epochs. By using Photogrammetric technics, DSM and orthophoto were generated using the Pix4D software and had been already registered by following the procedures from Aicardi et al., (2016).

1.2. Research Identification

There is a need for an automated approach for change detection using UAV images as it is currently not fully developed. Many types of research for change detection have been conducted using satellite images with different resolution. So, this research focuses on the automatic method for performing classification and change detection using DSM and orthophoto generated from UAV images. Different change detection approaches was used to understand how change detection using UAV images can better be performed. Three algorithms were used whereby the first algorithm uses DSM for height change detection, the second and the third algorithm uses orthophoto and DSM features for classification of changes which was based on the conditional random field model. Having eight images taken at different time, provide more data to be used as training samples, so training was done using the first four epochs, and another test was done by increasing the samples from each classified epoch to attempt improving the classification accuracy.

The performance of the algorithm was evaluated using accuracy assessment. Figure 1 and Figure 2 shows some of the orthophotos with its corresponding DSM for the first and the last epoch which was used as input for the algorithm. Data was acquired in different epochs at a construction area in Lausanne (Switzerland).

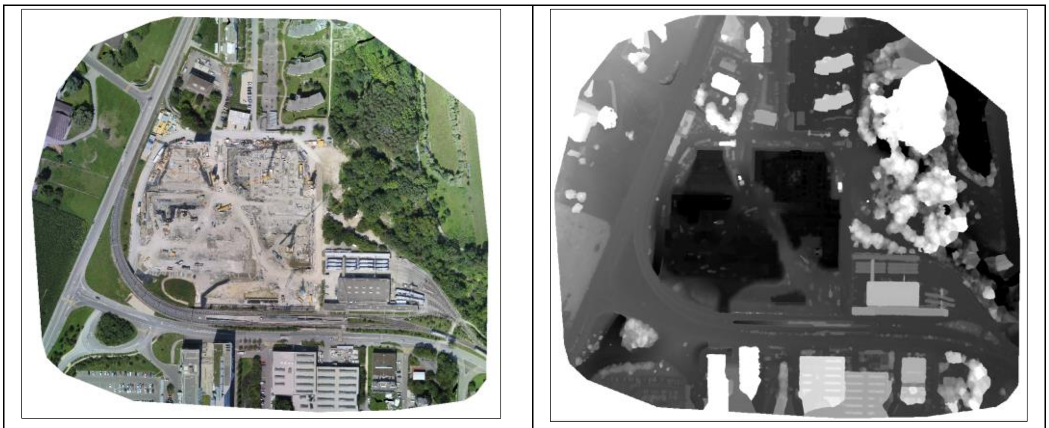

Orthophoto DSM

Figure 1: Orthophoto and DSM for the first epoch

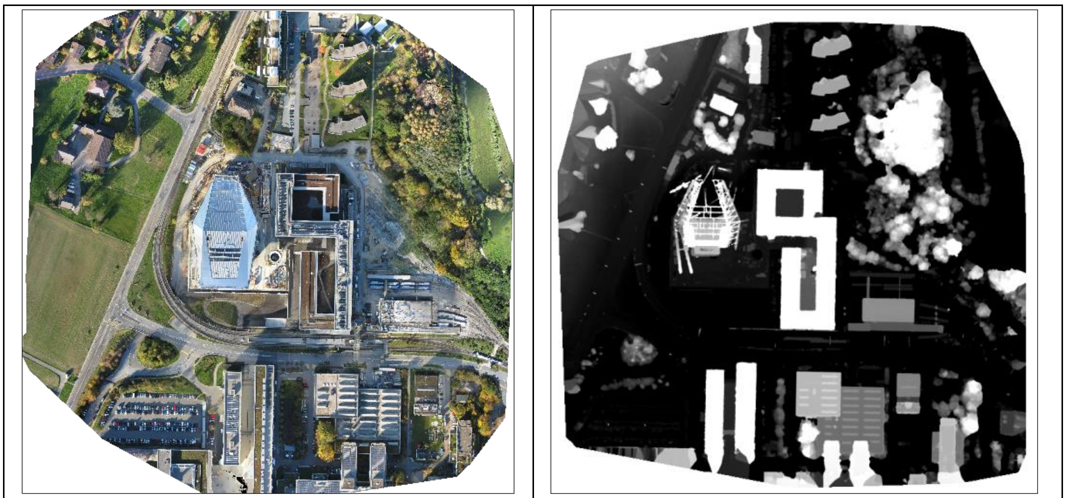

Orthophoto DSM

Figure 2: Orthophoto and DSM for the last epoch

1.3. Research objectives

The main objective of the research is to propose a reliable approach for automatic classification and change detection within a scene using DSM and orthophoto generated from UAV images.

The specific objectives are as follows,

1. Conducting a literature review on the state of art change detection techniques.
2. Develop a methodology for change detection with DSM as input.
3. Develop a methodology and algorithm for change detection based on CRF model with orthophoto and DSM features as input using two different techniques.
4. To test the performance of the new algorithm.

1.4. Research questions

Concerning the above mentioned objectives, the following research questions was addressed.

Specific objective 1

i. What are the available algorithms for change detection?

ii. What is the most suitable approach to define the unary and pairwise potential terms in the CRF-model?

Specific objective 2

i. Which is the best change detection technique using a DSM as input?
ii. How to use rule based to distinguish changed and unchanged DSM?
iii. How to smooth the false changes due to DSM noise?

Specific objective 3

i. How to define the training for four classes?
ii. How to compose the pairwise potential for DSM and orthophoto?
iii. What is the contribution of DSM and orthophoto in classification results?

Specific objective 4

i. What is the performance of the proposed algorithm using DSM and Orthophoto?
ii. How do fully connected CRF and random forest compared in terms of accuracy?
iii. Can accuracy be improved by adding the training sample from the classified epoch?

1.5. Innovation aimed at

This research seeks to develop the new algorithms for automatic change detection whereby DSM and orthophoto generated from UAV images was used as input and while refinement of the classification was done using CRF model. In literature, most of the change detection researchers use satellite images as input, and just a few of them use CRF-model for improving change detection in the area of interest. But also most of the researches do not combine 2D and DSM features. This research aims at testing the capability of CRF model in smoothening the classification results used for change detection using DSM and orthophoto from UAV images and define the typology of change (change with classes). Visual analysis of the orthophoto images and DSM change was used in collecting the reference data during the research and evaluating the accuracy assessment.

1.6. Thesis structure

Chapters of the thesis, Chapter one will cover the background and an introduction to the research including its motivation, research objectives, research questions, and the innovation to why the research must be done. Chapter two will cover the review of the related works that have been done in other researches including change detection techniques which have been used as well as the use of fully connected CRF. Chapter three will explain about data that was used in the experiment and the software that was used for data processing. Chapter four will explain a step by step of the method that was adopted during the implementation of data processing. Chapter five will contain the experimental results, and the discussion of the results will be done in chapter six. Chapter seven will contain the conclusion according to the obtained results, answers for the research questions and the recommendation for further studies.

2. LITERATURE REVIEW

This chapter will give an overview of the existing change detection techniques that have been conducted in different researches by comparing the results that they achieved and the conclusion they made. A brief review on the CRF will also be presented in this chapter.

2.1. Change detection methods

Change detection is the process of analysing the changes that have been taken place in the area within a specific period. The process of change detection requires a multi-temporal dataset (images acquired in the same area at the different time) (Campbell & Wynne, 2011). Change detection has been implemented using different methods, such as image differencing, principal component analysis, image rationing, post classification, pre classification just to mention few. However, some of the studies have also been conducted to compare their ability in analysing changes. Afify (2011) and Frauman E and Wolff E (2006) compares various change detection methods including image differencing, image rationing, principal component analysis, change vector analysis and post classification. From those studies, post classification change detection technique which also have the ability to classify changes into from-to classes was concluded to have more accuracy than other techniques.

Change detection studies have been researched using different dataset, whereby Bazi, Bruzzone, and Melgani (2005) conduct change detection using multi-temporal SAR images which are not used much due to the problem of suffering from speckle noise. The proposed algorithm involves image filtering to reduce the speckle noise before change detection.

Sarp et al. (2014) uses orthophoto and point cloud for building change detection. The approach consisting of three basic steps, classification using support vector machine, normalizing point cloud by taking point cloud generated from the aerial image and point cloud generated from topographic maps, the last step was determining the changes by comparison between before and after the earthquake event data. The authors make a comparison on the result obtained using orthophoto only, and the results obtained using orthophoto with normalized DSM (nDSM) and concluded that the use of nDSM improves the result.

Cao, Zhou, et al. (2016)use satellite images with 2.5m pixel resolution. The change detection method proposed based on CRF model. Unary and pairwise potential of the CRF was defined using fuzzy C-mean membership and a linear combination of the Gaussian kernel. Manually created ground truth map was used to check the accuracy of the output change map. The results (accuracy) of the proposed approach was compared with other methods as PCA-k-mean, traditional CRF, MRF and kernel method. The author concluded that the new proposed method has higher precision and does not consume too much time in processing compared to other methods.

All these studies use different approaches in terms of methodology on how to conduct the change detection and most of them analyse the results into change and unchanged classes. However all those change detection techniques lies in the two main types which have been mentioned by Dinand et al., (2013): (i) Algebra change detection which includes, image differencing, image rationing, image regression, vegetation index differencing, change vector analysis and background subtraction techniques and (ii) Classification based change detection techniques which include, hybrid change detection, post classification comparison, unsupervised change detection and spectral temporal analysis.

2.1.1. Algebra change detection

Algebra change detection is a pixel based change detection method. In algebra changes are detected pixel by pixel. The techniques include image differencing, image rationing, image regression, vegetation index differencing, change vector analysis and background subtraction techniques (Dinand et al., 2013). Despite the easiest of detecting changes, algebra change detection has some challenges. When using algebra change detection technique there is no information about the from-to change, it also requires a careful threshold selection as the change, and no change can only be differentiated using the given threshold (Lu, Mausel, Brondízio, & Moran, 2004). Among the mentioned algebra change detection techniques, image differencing has been used in many studies.

Image differencing

Image differencing is a pixel based technique whereby values from the same band on different images are used to create a change image (Théau, 2012). Before conducting image differencing, two images must be registered and have the same pixel size (İlsever & Ünsalan, 2012). The output of image differencing is zero when there is no change, and positive or negative when there is change. The big challenge of image differencing is on defining the threshold which will be used to separate the changed and unchanged area of the output. Another big challenge of image differencing technique explained by Lu et al., (2004) that it cannot provide a change matrix with many details. Equation 1 gives the outline of how image differencing change detection has been conducted.

$$I = Img_2(x, y) - Img_1(x, y) \qquad (1)$$

From the equation above, Img_2 and Img_1 are two images taken in two different time on the same area, I is change image generated after differencing of the value from pixel(x, y). Image differencing techniques have been applied in change detection when using DSM as is the straightforward way of doing that and easy of output interpretation. In DSM only height information is present in each pixel, so when doing change detection using image differencing method it is only the subtraction of the height from the pixel of one DSM to another DSM (Hong, Jianqing, Zuxun, & Zhifang, 1999; Z. Liu et al., 2003; Xu et al., 2015; Xuan, 2011).

2.1.2. Classification based change detection

Classification based change detection techniques involve all kind of change detection that uses classification of either separate image or combined images. These category includes post classification change detection, hybrid change detection, pre classification change detection, spectral temporal analysis and unsupervised change detection just to mention few of them.

Post classification change detection

Post classification change detection technique is the most popular method which lays in the category of classification based change detection (Dinand et al., 2013). Post classification consist of classification of images captured in different time followed by the overlay of those images and analysing the class change from one classified image to another (El-Hattab, 2016). Post classification can be supervised or unsupervised depending on the presence of reference data for the area to be analysed (H. Liu & Zhou, 2010).
However, supervised change detection has an advantage in providing the qualitative (change map) and quantitative (change statistics) for the analysed images. Unsupervised change detection can also be conducted due to the lack of data to be used as a base information or reference data (Ghosh, Mishra, & Ghosh, 2011; Leichtle, Geiß, Lakes, & Taubenböck, 2017). Quantitative information will help in knowing the amount of area that has been changed as well as knowing the area with false changes and true changes. Though post classification change detection suffers from error propagation from the classification output, still it is the method that has been used by many researchers (Afify, 2011; H. Liu & Zhou, 2010; C. Wu, Du, Cui, & Zhang, 2017).

Post classification change detection techniques have an advantage of providing the change information as from which class a pixel has changed. Change information can be interpreted using the change matrix which shows what have been changing between two dates (Théau, 2012). Post classification requires sufficient training sample during the training of the classifier to have a good classification accuracy. The final accuracy of the change detection depends on the accuracy of the individual classified images used as input (Lu et al., 2004).

Pre classification change detection

Not only post classification but also pre classification change detection technique lies in the classification based change detection technique. Pre classification change detection technique consisting of analysing the changes by overlaying the feature values pixel by pixel from one epoch to another (Peiman, 2011) followed by interpretation and classification of those changes. Frauman E and Wolff E (2006) explains that the quality of the output from pre classification change detection technique depends mostly on the quality of the image used as input. And with a comparison to post classification method, pre classification has been explained as the fastest way of visualising changes though it needs a lot of time for interpretation.

2.2. Classification

Digital image composed of a number of pixels in which some of them are related, and others are different due to the variation of spectral properties in the image. These image pixels are grouped according to their spectral properties. The process of grouping image pixels to their respective classes according to some given properties is called image classification (Campbell & Wynne, 2011). Pixels grouped in one class appeared to have similar features than pixels grouped in another class. The classification is categorized into two methods: (i) supervised and (ii) unsupervised classification. Each classification method has its advantage and disadvantage.

The unsupervised classification method is normally applied when there is no training sample in the area to be classified. In this method, the classification based on grouping the pixels with similar spectral values in the image according to some given rules. Due to the availability of the data, these approaches are very often difficult to handle as the threshold and the rules set can vary from one case to another case.

Supervised classification can be conducted when there is the availability of training samples (ground truth) of the area to be classified. These samples can be used during training of the classifier on defining how the pixels are assigned to a certain class. Availability of reference data makes easy to detect the errors due to misclassification through confusion matrix. Reference data and the classification output can be compared, and the classification matrix to be produced. Independently from the used classifier, the ground truth is mandatory to assess the performance of the classifier.

Some of the common used classifier for very high resolution images classification includes Support Vector Machine (SVM) (Adam, Mutanga, Odindi, & Abdel-Rahman, 2014; Otukei & Blaschke, 2010; Pal & Mather, 2005; Sesnie, Finegan, & Gessler, 2010), Maximum Likelihood Classifier (MLC) (Otukei & Blaschke, 2010) and random forest, which is termed as decision trees (Adam et al., 2014; Chehata, Guo, & Mallet, 2009; Fan, 2013; J. Liu, Feng, Gong, Zhou, & Li, 2016; Sesnie et al., 2010).

2.2.1. Conditional Random Field (CRF)

The conditional random field is a classification/segmentation technique that takes into consideration the use of contextual information in producing the better classification results. Lack of contextual information during classification results into the noisy classified image, especially for the very high resolution images. High resolution image classification is a very big problem in the process of image analysis due to the availability of a lot of information on it (Sun, Lin, Shen, & Hu, 2017). From that perspective, there is a need for a very powerful classifier. But still, the result will not be as good as it is supposed to be. The conditional random field is then used to smoothen the classification output (Sun et al., 2017). Most of the classifier gives a class label to a pixel without making consideration of the neighbourhood information from another pixel. Conditional random field takes into consideration the relationship between the pixel label and the nearby pixels regarding colour information as well as the position between the pixels.

The conditional random field can be divided into two part; (i) Unary potential and (ii) Pairwise potential. The unary potential is the term which represents the relationship of the pixel label and the observed data, and the pairwise potential is the term which represents the relationship of the pixel label, its neighbour and the observed data. The general CRF as explained by Li and Yang (2016) can be defined as shown in Equation 2.

$$E(X) = \sum_{i \in V} \emptyset_{\boldsymbol{i}}(\boldsymbol{x_i}) + \sum_{(i,j) \in N} \emptyset_{\boldsymbol{ij}}(\boldsymbol{x_i}, \boldsymbol{x_j}) \quad (2)$$

From the above equation, unary potential is given by $\emptyset_{\boldsymbol{i}}(\boldsymbol{x_i})$ and pairwise potential is defined by $\emptyset_{\boldsymbol{ij}}(\boldsymbol{x_i}, \boldsymbol{x_j})$. The CRF general equation can then be expanded in terms of their normalization constant and potential function as it is shown in Equation 3.

$$p(y|x;\theta) = \frac{1}{Z(x;\theta)} exp - \left\{ \sum_{i \epsilon s} \emptyset_i(y_i, x; \theta_u) + \sum_{i \epsilon s, j \epsilon \delta_i} \emptyset_{ij}(y_i, y_j, x; \theta_p) \right\} \quad (3)$$

From the above equation, $\emptyset_i(y_i, x; \theta_u)$ is unary potential, $\emptyset_{ij}(y_i, y_j, x; \theta_p)$ is pairwise potential, $Z(x;\theta)$ is a normalization constant and δ_i is the local neighbourhood for pixel s (Zhou, Cao, Li, & Shang, 2016).

2.2.1.1. Unary potential – classification algorithms

The unary potential is the model which represent the relationship between the class label and the data/observation. The unary potential is computed for each pixel which is the probability of assigning a label to a particular pixel. Equation 4 from the paper written by Li and Yang (2016) explains that unary potential is in the form of negative log likelihood which is the conditional probability density that is used to minimize the function.

$$\emptyset_i(x_i) = -logP(x_i|I) \quad (4)$$

The unary potential defined in Equation 4 can be individually computed from the chosen classifier (Yang & Förstner, 2011a). However variety of classifiers can be used to define the unary potential of the CRF including Textonboost classifier (Li & Yang, 2016), Fuzzy-C-means classifier (Cao et al., 2016; Zhou et al., 2016) and random forest (Sun et al., 2017; Yang & Förstner, 2011).

In this research unary potential was defined using the random forest as it has been termed as the robust classifier and gives good classification results by Yang and Förstner (2011). The random forest can handle large dataset with higher computational load and still produce good results (Chehata et al., 2009; Sun et al., 2017). However random forest has been compared with other classifiers like SVM, MLC and found to perform better (Feng, Liu, & Gong, 2015; J. Liu et al., 2016; Sesnie et al., 2010; Sun et al., 2017).

Random forest

Random forest is a classification method consist of a combination of decision trees which are termed as a weak classifier (individually) and form a strong classifier introduced by Breiman (2001). Training pixels can be randomly selected and returned to the set which makes it possible for the training to be used more than once in training the trees to form a forest. The advantage of using random forest classifier is that each classification tree produces its individual error, but when combining all the number of trees used the classifier become more powerful, and hence better classification output. Another advantage compared to other machine learning classifiers such as CNN and SVM is using less time during training (Na, Zhang, Li, Yu, & Liu, 2010). The random forest has a strategy of using set of the trees to predict the class of the pixel, and the class which will be predicted by the majority will be assigned to the respective pixel (Sun et al., 2017) as shown in Figure 3.

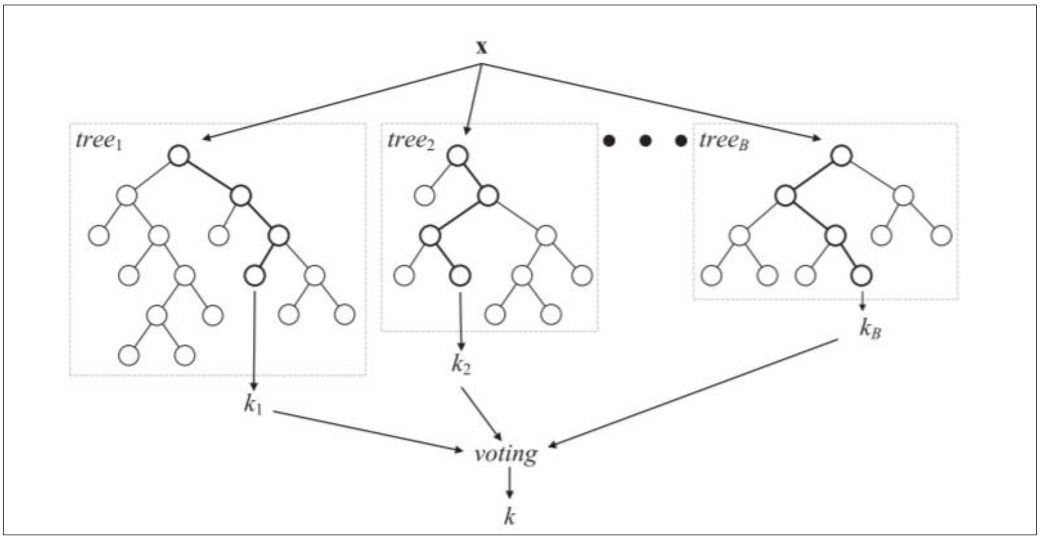

Figure 3: Random forest architecture (Verikas, Gelzinis, & Bacauskiene, 2011).

The random forest has been used in many studies to define the unary potential of the CRF. Sun et al., (2017) decide to use the random forest for solving the problem of handling a large number of training samples. Another study done by Yang and Förstner (2011b) claims that they decided to use the random forest as it is a good classifier for façade classification tasks.

2.2.1.2. Pairwise potential

The unary potential can be produced from the classifier by giving the pixel label based on the interested pixel which mostly contains noise. The pairwise potential which makes use of the contextual information available in the input image can be used to smooth those noise. Pairwise potential defines how the pixel is related to their neighbour pixels (Cao et al., 2016). The relationship can be a short range which includes 4 connected CRF or 8 connected CRF and long range which include fully connected CRF as it can be seen in Figure 4. In fully connected CRF a pixel label is defined by finding the relationship between the interested pixel and all the pixels in the image.

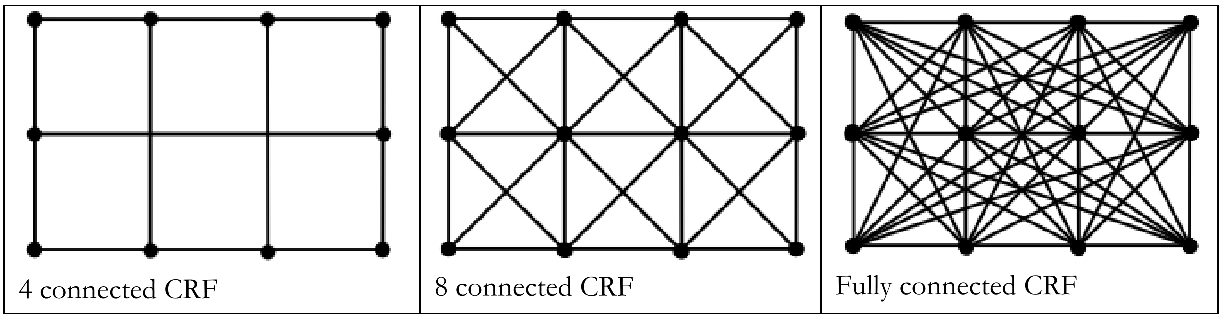

Figure 4: Representation of short range CRF (4 connected CRF and 8 connected CRF) and long range CRF (Fully connected CRF) (Li & Yang, 2016).

Fully connected CRF

Krähen and Koltun (2011) were the first to introduce fully connected CRF whereby a pixel label was defined using all the pixels in an image. Fully connected CRF make use of the contextual and positional information in defining the label of the pixel of interest. As explained by Krähen and Koltun (2011) pairwise potential for the fully connected CRF is defined as shown in Equation 5.

$$\emptyset_{\boldsymbol{ij}}(\boldsymbol{x_i}, \boldsymbol{x_j}) = \mu(x_i, x_j) \sum_{m=1}^{K} w^{(m)} k^{(m)}(f_i, f_j) \tag{5}$$

Whereby μ is the label compatibility function, $w^{(m)}$ is the weight of the Gaussian function and $k^{(m)}$ is the Gaussian kernel consisting of appearance kernel and smoothness kernel (Krähen & Koltun, 2011). The smoothness kernel (Equation 6) is used to remove the small pixels that appear to be isolated from other class labels. The appearance kernel (Equation 7) is based on the nearby pixels that have the same RGB/colour properties that are termed as they belong to the same class.

$$k^{(1)}(f_i, f_j) = w^{(1)} \exp\left(-\frac{|p_i - p_j|^2}{2\theta_\gamma^2}\right) \tag{6}$$

$$k^{(2)}(f_i, f_j) = w^{(2)} \exp\left(-\frac{|p_i - p_j|^2}{2\theta_\gamma^2} - \frac{|I_i - I_j|^2}{2\theta_\beta^2}\right) \tag{7}$$

From Equation 6 and Equation 7 above, p_i and p_j are positional vectors, I_i and I_j are a colour vector. Colour vector is defined by the RGB colour space, with the assumption that the same colour pixels belong to the same class label. The positional vector used to smoothen the results by removing small particles which appears as they are isolated.

Krähen and Koltun (2011) also propose the use of mean field inference which minimizes the energy function. Mean field does not compute the exact distribution of image pixels. Instead, it computes the distribution that minimizes the KL-divergence of all the distributions to be defined as independent marginal. After the introduction of the fully connected CRF, it has been applied in many studies and found to give good results with better accuracy (Krähen & Koltun, 2011; Li & Yang, 2016; Sun et al., 2017).

2.2.2. Accuracy assessment

Accuracy assessment is one of the measures of the correctness of the output compared to the reference data. For classification purpose, if the classified image is somehow similar to the reference data it is termed to be more accurate (Campbell & Wynne, 2011). Accuracy can be measured using several methods including overall accuracy (Afify, 2011; Gevaert, Persello, Sliuzas, & Vosselman, 2017), intersect over union (IoU) score (Marin-Jimenez, Zisserman, Eichner, Ferrari, & Ferrari, 2013), precision (Davis & Goadrich, 2006; W, 2011) and kappa analysis (Afify, 2011; C. Wu et al., 2017). However, some of the change detection studies use visual inspection by comparing the change polygon with the reference data (Okenwa, 2016).

3. DATA AND SOFTWARE

This chapter will give a description of the data and the software used for preparation and processing of the provided data during the research.

3.1. Data description

The dataset used was the orthophoto and DSM generated from UAV images acquired in the construction area in Lausanne (Switzerland) with approximate of 32,830m^2. The image was acquired in eight different epochs using UAV, and they were processed using the Pix4D software for orthophoto and DSM generation. The UAV image acquired with a sampling distance of 5cm. Due to the high resolution of the dataset, a lot of information is available on the images. Four classes were identified from the orthophoto: road (road, railway), buildings (roof and concrete), vegetation and bare soil.

3.2. Software

Image preparation was done using ERDAS imagine a software, whereby an area of interest was generated to ensure that there is a common area used for all of the epochs. The common area was selected because area coverage for each epoch was not the same.
By using ENVI 5.3 + IDL 8.5 software, the ground truth for all of the epochs was generated, with the total of four classes. Since the output from ENVI software was shapefile and cannot directly be opened in Matlab for further processing, it was imported into the ArcGIS 10.5.1 software to produce the raster format for further analysis using Matlab R2016a programming software.

3.3. Reference data

The subset created was used for ground truth generation of each epoch. By visual inspection, the ground truth for orthophoto was generated. Original images with their corresponding ground truth can be seen in Figure 5.

Epoch	Orthophoto	Ground truth
1		

2		
3		
4	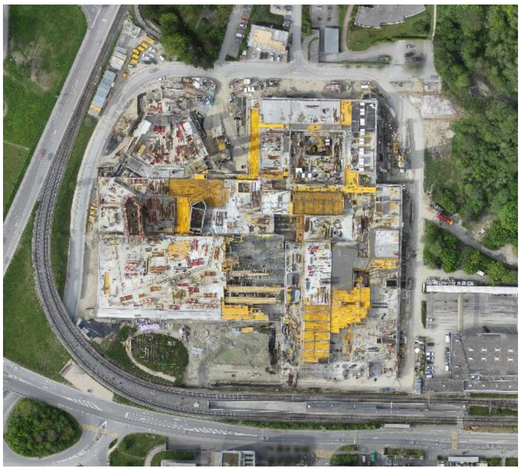	

5	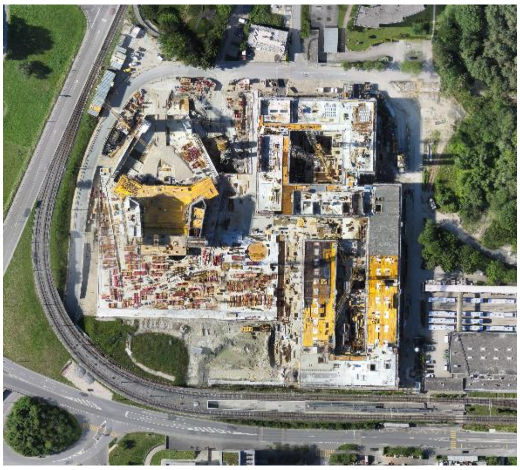	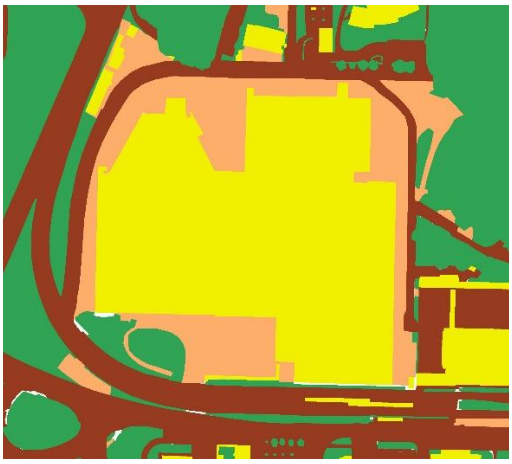
6		
7	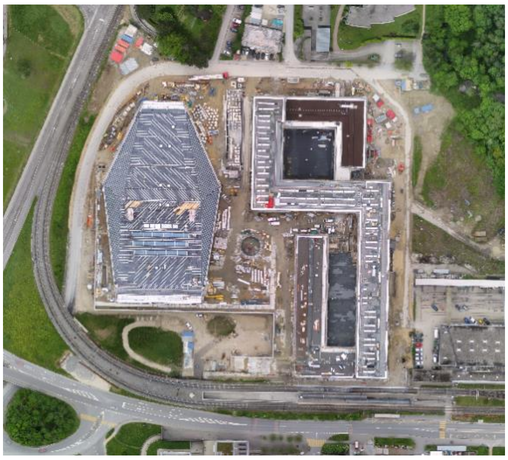	

8		
	Vegetation Road Building Bare soil	

Figure 5: Orthophoto images with their corresponding ground truth

Ground truth was also generated using DSM changes. Using Envi software, two DSM of the consecutive epochs was overlaid one another, and by visual inspection, the change in height was digitized as it is shown in Figure 6.

Epoch t	Epoch t+1	Ground truth for DSM changes
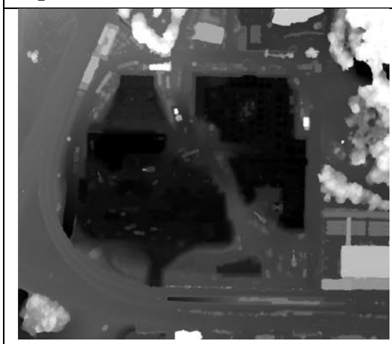 DSM 1	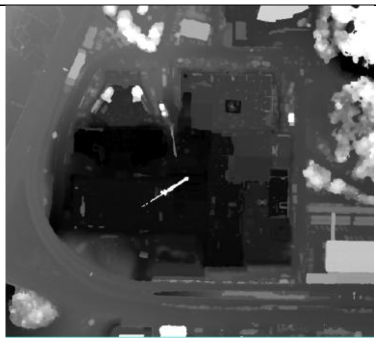 DSM 2	 Change 1
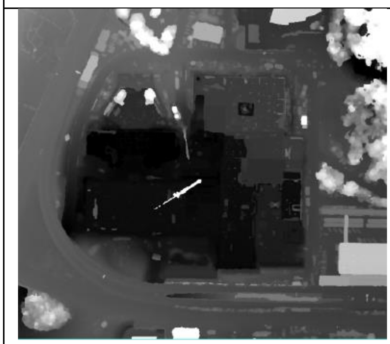 DSM 2	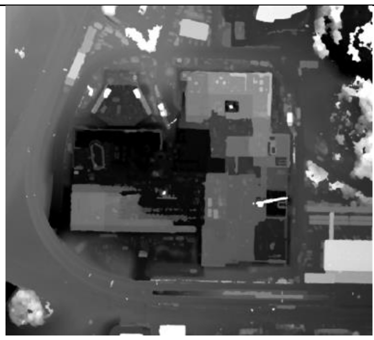 DSM 3	 Change 2

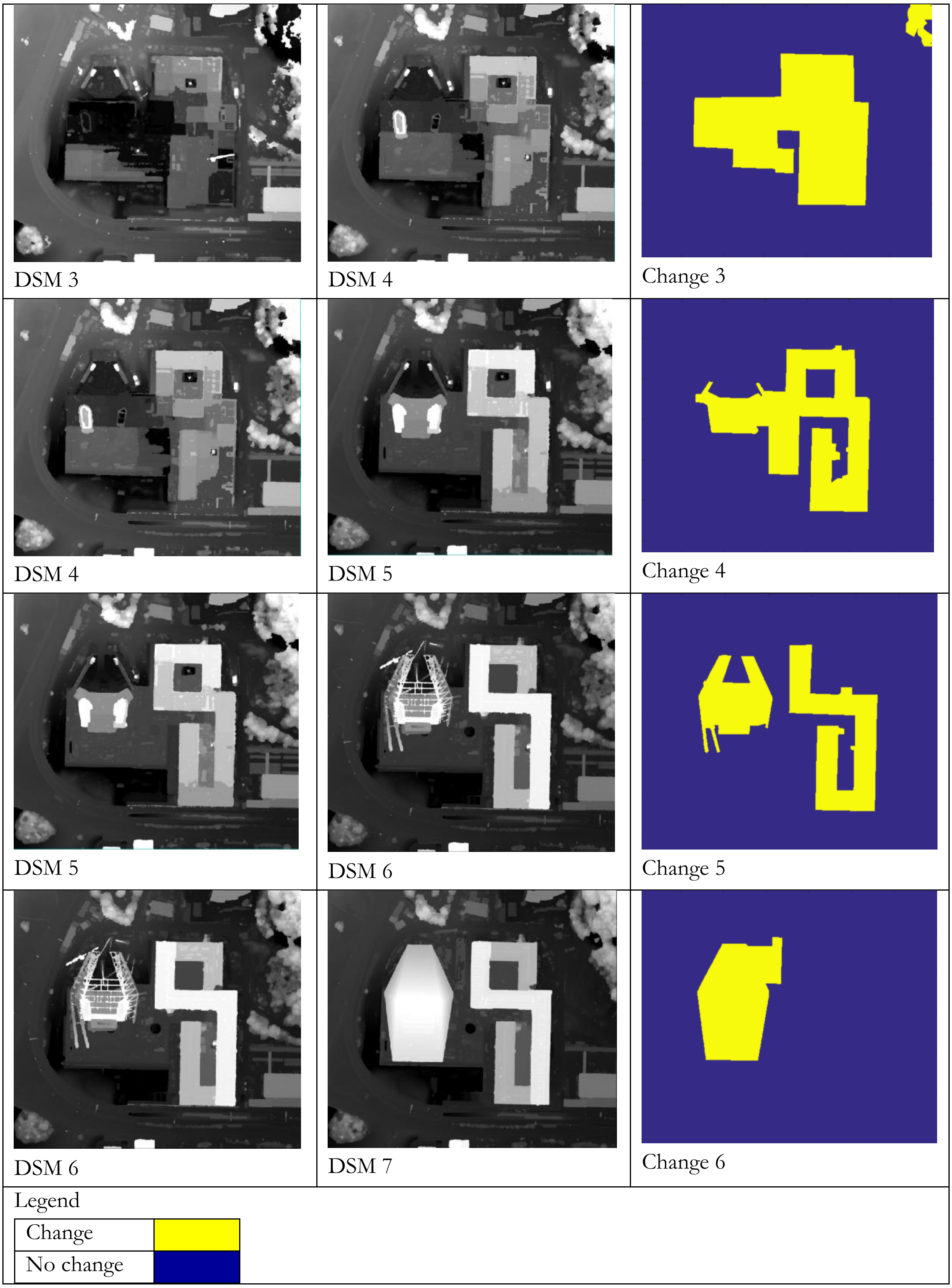

Figure 6: DSM's and their corresponding DSM change ground truth

4. METHODOLOGY

Chapter 4 will give a step by step explanation about the methods selected for doing classification and change detection of the DSM alone and the DSM with orthophoto, and how the experiment was conducted for better results.
Three different approaches used during the implementation of this research. DSM change detection was the first one to be implemented whereby image differencing technique was used to detect height change between two epochs. Post classification change detection was the second approach whereby a change from one class to another was detected. And lastly, the pre classification change detection was conducted whereby change between features identified first followed by the classification of changes. All these approaches are explained one by one in the following subsections of this chapter.

4.1. DSM change detection

DSM change detection was done using image differencing change detection technique. Since DSM contains only the height information for each pixel, the best way of doing change detection was pixel by pixel height differencing. Figure 7 shows a step by step implementation of DSM change detection which start by height differencing. Thresholding was next step to separate between the changed pixels and unchanged pixel followed by smoothening the changes to removing noise.

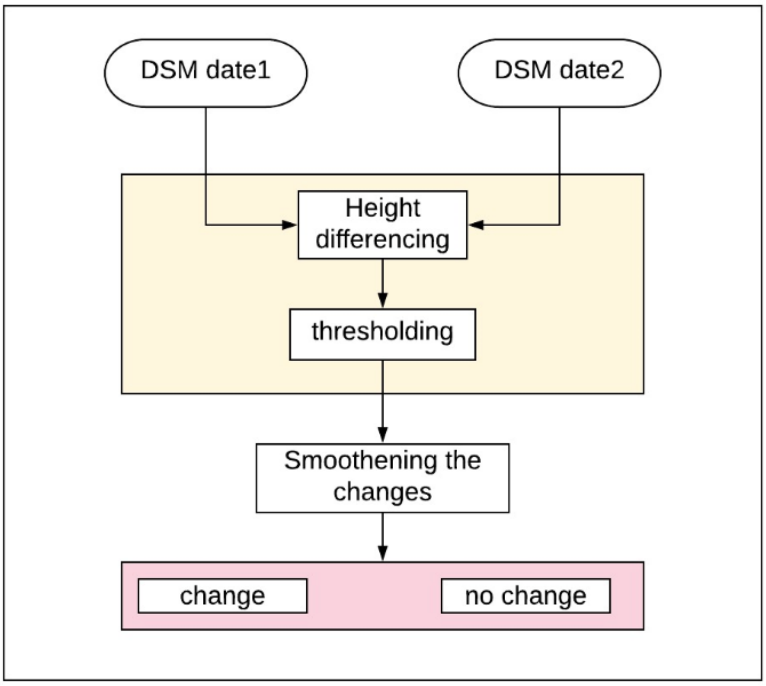

Figure 7: DSM change detection workflow

4.1.1. Height differencing

Change detection for the DSM was computed by height differencing. From the height of a pixel in DSM of date 1 and the same pixel in DSM of date 2, a height change of a particular pixel was determined and used to generate a new change map. The generated change map consists of different values which are then confusing in determining the changed and unchanged area. This problem was solved by the thresholding process as explained in the next subsection.

4.1.2. Thresholding

Thresholding was used to identify the changed area and unchanged area of the DSM change output. Thresholding of the DSM change was done as the supervised way of detecting the changed and unchanged part. A threshold was selected, and all values below the selected threshold termed as the unchanged part, and the value above the threshold termed as the changed part of the two epochs used. The threshold value was selected by visual analysis of the output and the accuracy obtained after generation of confusion matrix using the ground truth for DSM change. About three different thresholds were tested.

4.1.3. Smoothening of the DSM change

DSM change was smoothed using the mathematical morphological operation opening. The opening consists of two operations which are erosion followed by dilation. Erosion was used to remove the small/isolated areas using the defined structuring element, and dilation was used to expand the area using the same structuring element (Persello, 2017; Q. . Wu, Lu, & Ji, 2009). The mathematical morphological operations work only on the binary images, which makes it easy to use in the DSM changes. By using erosion, small areas was removed, and other areas was shrunk according to the defined structuring element. Dilation was used to restore the shrunk part of the binary image to its original before using erosion which results in an image somehow free from noise.

4.2. Post classification change detection

Post classification change detection method consists of overlaying the classified map one to another and detecting the changes from them as it can be seen in Figure 8, which shows the workflow of post classification change detection method. The changes to be detected are the class change. Post classification consisting of extracting 2D and DSM features for classification followed by definition of the unary term and pairwise term to smoothen the result. Overlaying of the classified image from two different epochs which produce change map.

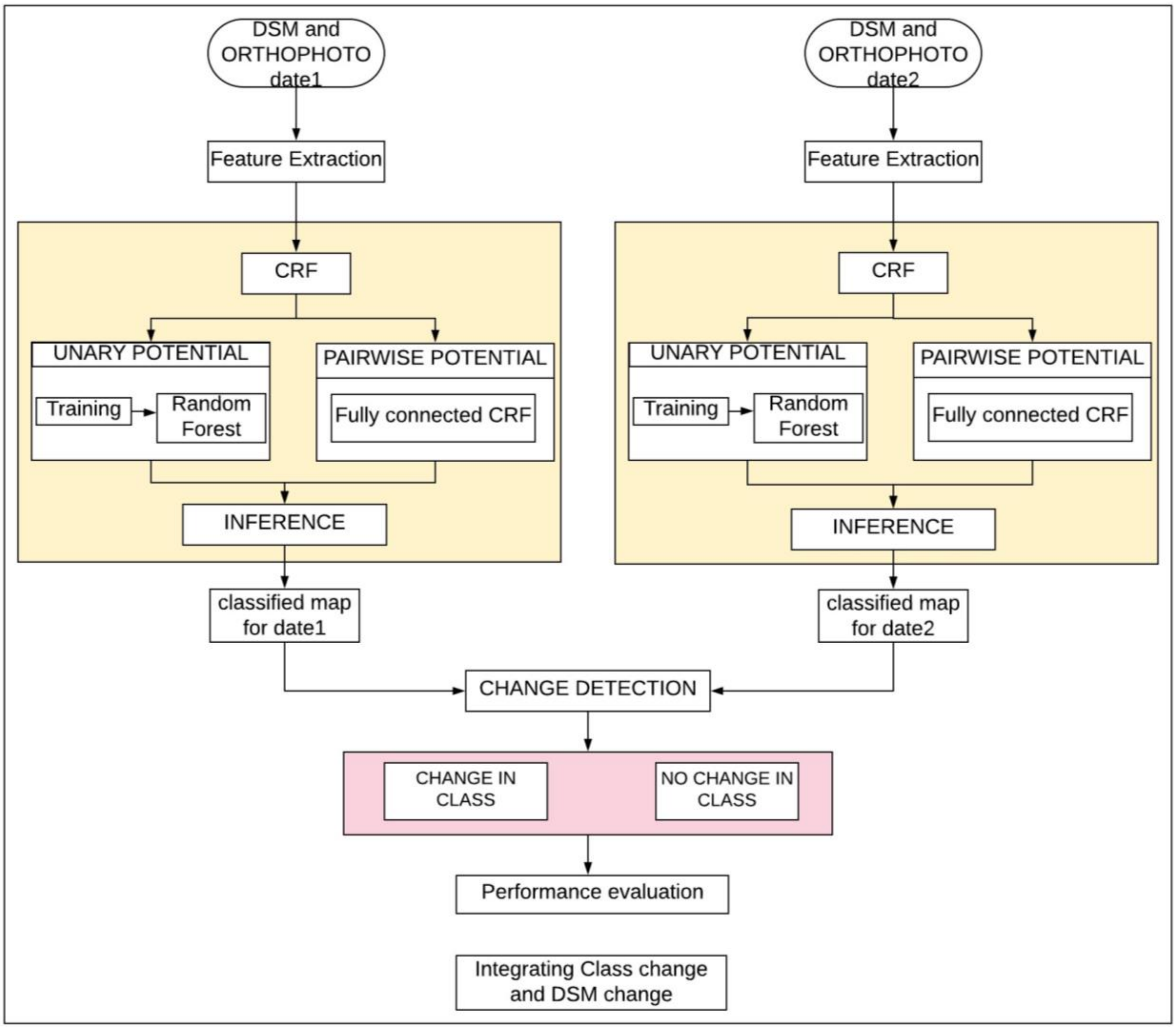

Figure 8: Post classification change detection workflow with yellow presenting the classification using CRF and pink representing the results of change detection

4.2.1. Feature extraction

For the classification purposes, features were extracted from orthophoto and DSM as well. From the orthophoto spectral features and textural features was extracted and from DSM geometrical features was extracted. Spectral features extracted was HSV features, GLCM features for textural features and planarity and linearity features as geometric features were extracted from DSM.

4.2.1.1. HSV features

HSV are colour features which extract three types of information from RGB colour. The information extracted are hue, saturation and value. S. Wu et al., (2015) explains that colour features are one of the fundamental quality of the image and HSV colour space as it is mostly used for image analysis and gives higher accuracy in image classification than RGB colour space. Hue represents the original colour of an object if it is yellow, blue, or red, saturation represent how an original colour was diluted in the white colour, and value describes the colour brightness (Hamuda, Mc Ginley, Glavin, & Jones, 2017). HSV features obtained by converting the RGB colour space into HSV colour space whereby hue ranges from 0 to 360, saturation and value presented by percentage.

4.2.1.2. GLCM features

Textural features as described by Haralick, Shanmugan and Distein (1973), are features which have spatial distribution information of tonal variations within an image. Textural features categorized as being fine, coarse, smooth, rippled, mulled, irregular or lineated. The common method for textural feature extraction is by using grey level co-occurrence matrix (GLCM) (Mohanaiah, Sathyanarayana, & Gurukumar, 2013). The RGB image was converted into grey image followed by computation of co-occurrence matrix which is used for computation of textural features. The textural features used in this research are contrast, correlation, energy, dissimilarity, angular second, mean, variance and homogeneity. These textural features were extracted using ENVI software, and some of them are in presented in Figure 9.

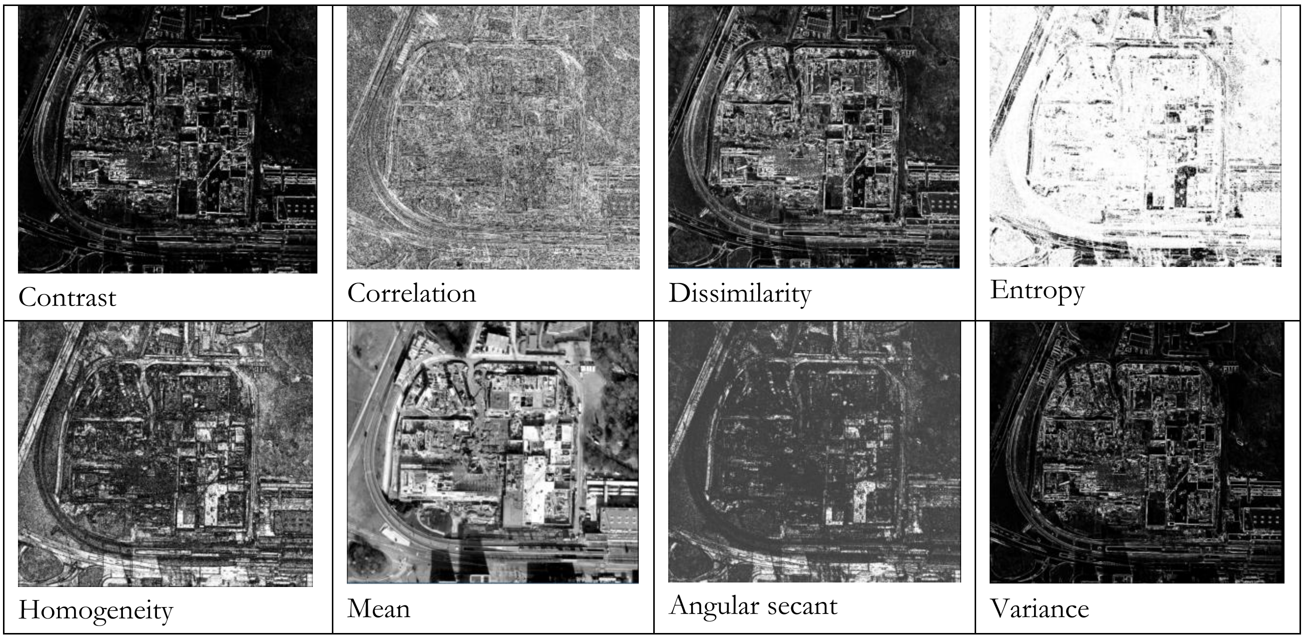

Figure 9: Extracted GLCM features for epoch three.

Contrast gives the local variation of a pixel with a comparison to its neighbour for the whole image. For the constant image, the contrast is 0. Correlation measures how the pixels relate to their neighbour for the whole image. The correlation value is from -1 to 1, whereby 1 represent the positively correlated image and -1 represent the negatively correlated image. The angular second moment which also termed as energy gives the sum of squared elements in the matrix, it ranges from 0 to 1. Homogeneity provides the measure for the closeness of the distribution of the elements in an image. The entropy features measures how grey level distribution is uniform in the image. The area which is homogeneous in the image is expected to have high entropy than the areas which are not homogeneous.

4.2.1.3. Geometric features

The geometric features extracted from DSM are linearity, planarity and normalised DSM (nDSM). Planarity and linearity features can be computed from eigenvalues within the local neighbourhood, and they describe spatially local distribution of the height pixels in DSM (Chehata et al., 2009). Planarity features show high values for planar objects and low values for non-planar objects. For an object to be planar, all its points must be on the same plane. Linearity features show higher values for linear objects and low values for the nonlinear object. Similar here, for an object to be linear all of its points must be on a straight line. The nDSM have been calculated by finding the minimum height value in the DSM and subtracting all the height pixels from the minimum height value.

4.3. Conditional random field

A conditional random field consisting of the unary potential and pairwise potential. For this research, the unary potential was defined using the random forest, and the pairwise potential was defined using fully connected CRF.

4.3.1. Random forest

The classification was conducted using random forest classifier. From the total of eight epochs, four of them was used to train the random forest classifier, and the remaining four was used to test the classifier. A total of fourteen features used for classification purposes including 2D (orthophoto features) and DSM (Geometric features).
In random forest number of trees to be computed must be defined. For this research 30 trees were used in computing the classification model which takes more than one hour of training. Out of bag error estimation was also computed during the training of the random forest. The out of bag estimation was used to monitor the classification error as explained by Breiman (2001).
The output from the random forest was the probability of each class in a pixel. This research had four classes, so the output was each pixel having four different probability from each class, and the higher probability was considered to be the dominant class at that particular pixel. This lead to a lot of noise in the output of the random forest classifier.

4.3.2. Fully connected CRF

The results from random forest classifier was then refined using fully connected CRF model. Random forest classifier provides the individual pixel label without taking into consideration of the nearby pixels. Fully connected CRF (Krähen & Koltun, 2011) make use of the contextual information to refine the classification results from the random forest. Appearance and smoothening kernels of fully connected CRF are the ones used to refine the classification results by removing the isolated pixels and putting the nearby pixels in one class.
The parameters for the fully connected CRF which are the Gaussian kernel for appearance and smoothening was defined using the RGB standard deviation and x, y standard deviation respectively. These parameters are used to increase or decrease the long range connection of the fully connected CRF as explained by Krähen and Koltun (2011). For good classification results, parameters were fine-tuning to have the best set which provides higher accuracy.

4.3.3. Change detection

After a successful classification of the four epochs, the next step was detecting changes whereby the two classified epoch was overlaid pixel by pixel, and the change was detected from the overlaid image. Since we have four classes from the classification results, so the output was expected to have 16 classes as shown in Table 1. From the listed type of changes expected to occur, most of them were due to misclassification error.
However, a lot of changes in class appeared in the first three epochs which were used for training the classifier than the epochs used for testing. Still, change in height was seen in the DSM change as the building continued to be constructed from one floor to another. In the post classification change detection technique, the accuracy of the change detection depends mostly on the classification of the individual epoch. Due to the similarity of the spectral properties in some classes like building and bare soil, leads to misclassification of those classes and hence poor change detection accuracy.

Table 1: List of classes and change classes

classes	Change classes
Road	Road Road - building Road - vegetation Road - bare soil
Building	Building Building - road Building - vegetation Building - bare soil
Vegetation	Vegetation Vegetation - road Vegetation - building Vegetation - bare soil
Bare soil	Bare soil Bare soil - road Bare soil - building Bare soil - vegetation

4.4. Pre classification change detection

The last change method implemented was pre classification change detection. The workflow of this approach was somehow similar to the workflow of post classification change detection. From the workflow in Figure 10, the only difference is that change detection was done first followed by classification of those changes.

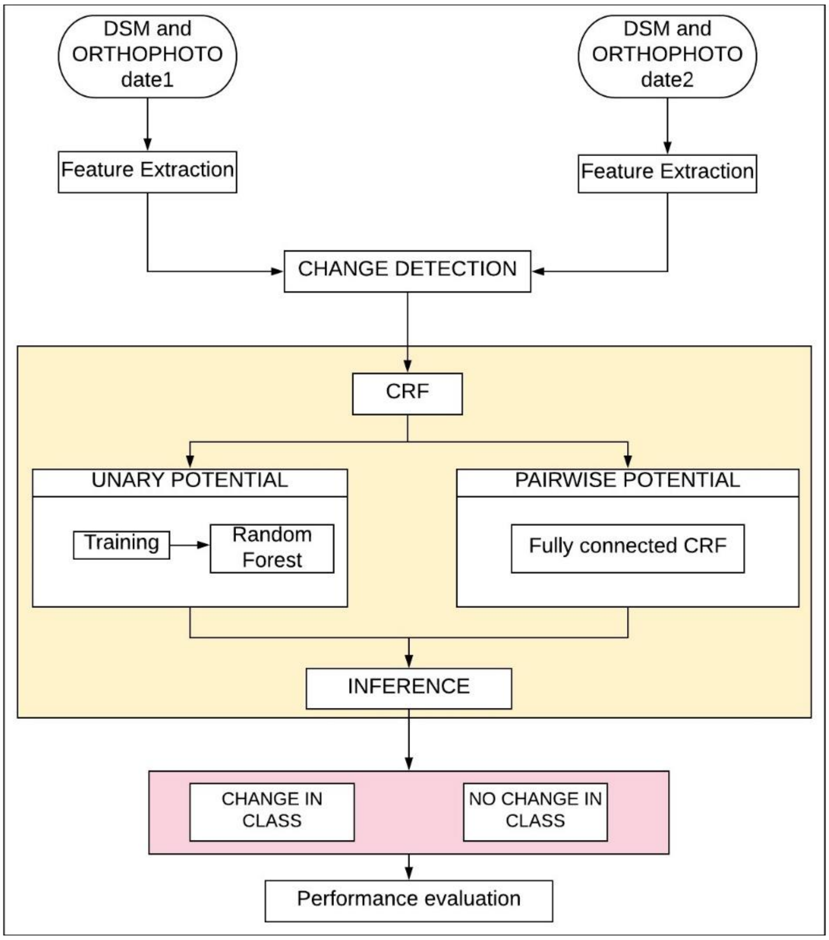

Figure 10: Pre classification change detection workflow with yellow presenting the classification using CRF and pink representing the results of change detection

The features used was the same as the one used in post classification change detection. These features are HSV, GLCM, planarity, linearity and nDSM. Feature extraction followed by change detection between those features. Classification of change features was the next stage, whereby CRF model was used. The unary potential for CRF was defined by random forest, and the pairwise potential defined by fully connected CRF.

4.5. Accuracy assessment

The accuracy evaluation was done using confusion matrix for both classification and change detection results. The accuracy assessment was computed by overall accuracy and intersect over union score. To have the accuracy assessment, the ground truth data and the predicted/classified output were needed for the comparison and checking the performance of the classifier. Intersect over union, and overall accuracy measures are computed using Equation 8 and Equation 9 respectively.

$$IoU = \frac{Area\ of\ overlap}{Area\ of\ union} \tag{8}$$

$$OA = \frac{\sum TP}{\sum all\ pixels} \tag{9}$$

Whereby area of overlap and area of the union are defined in Equation 10 and Equation 11 respectively.

$$Area\ of\ overlap = TP \tag{10}$$

$$Area\ of\ union = TP + FP + FN \tag{11}$$

From Equation 8, an area of overlap, an area of union are computed from the confusion matrix generated using classification output and the digitized reference data. From equation 10 and 11, TP (true positive) means the cases that were correctly classified, FP (false positive) means the negative pixels that were incorrectly classified as positive pixels, FN (false negative) means the negative pixels that were correctly classified as negative (Blomley, Weinmann, Leitloff, & Jutzi, 2014).

4.6. Integrating the DSM change and the class change

As the additional step in this thesis, the DSM change and the class change was combined to have a clear understanding of how the building changed from the initial stage of the construction. For the kind of data set used most of the changes appeared in height. The class change was mainly in the first three to four epochs, but height change can be observed in all the epochs. By integrating this information a clear understanding of how the changes have been taking place was conveyed.

5. RESULTS AND ANALYSIS

This chapter will present results from the conducted experiment that will help in answering the research questions. The results presented here will be for DSM change detection, post classification change detection and pre classification change detection. Some of the output including confusion matrix are presented in the appendix. The last section of this chapter will try to combine DSM change detection, and the outperform classification based change detection method to understand the relationship between them and how can they be used together.

5.1. DSM change detection

Change in DSM was done using image differencing technique, whereby the height of a pixel from DSM of one epoch was subtracted from a height of a pixel on DSM of the next epoch. Thresholding of 0.3m, 0.5m and 1m was manually selected to distinguish between the change and unchanged pixels. By using the ground truth for DSM change, the accuracy assessment was conducted to decide on which threshold value outperform others. Figure 11 shows DSM change for epoch 1 and epoch 2 with different thresholding values and their accuracy, other DSM changes will be found in Appendix A.

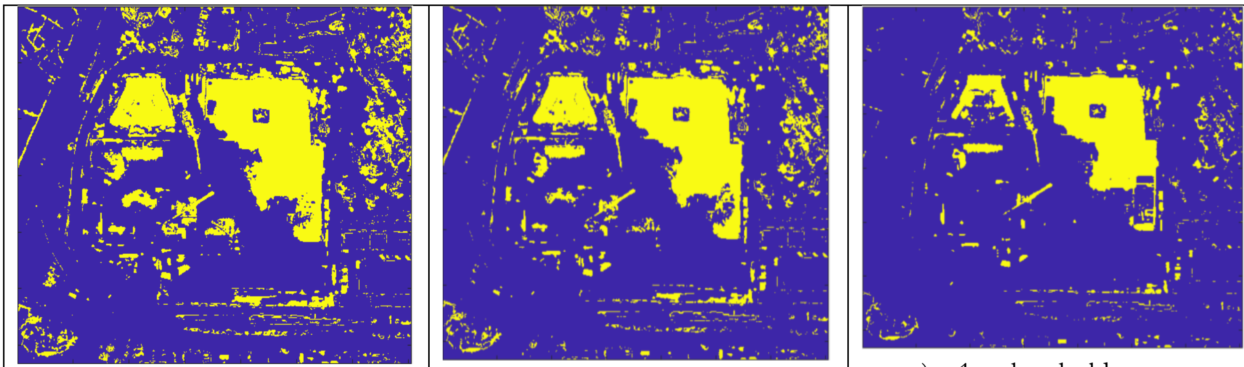

a) 0.3m threshold, OA=86.6%

b) 0.5m threshold, OA=89.5%

c) 1m threshold, OA=94.5%

Figure 11: DSM change detection for epoch 2 and epoch 1 using different thresholding with their overall accuracy.

The overall accuracy in percentage for the DSM change detection for all the eight epochs shown in Table 2, and the confusion matrix for this accuracy are presented in Appendix B.

Table 2: The overall accuracy of the DSM change in for three different thresholding

Thresholding	0.3m (%)	0.5m (%)	1m (%)
Epoch2-epoch1	86.6	89.5	94.5
Epoch3-epoch2	77.3	83.4	92.1
Epoch4-epoch3	80.3	83.6	87.8
Epoch5-epoch4	84.8	87.1	91.6
Epoch6-epoch5	84.7	88.2	92.1
Epoch7-epoch6	79.5	85.7	92.1

Thresholding of 1m was found to give more accuracy than the others and also improve visualization by removing a lot of noise. For DSM change, the changes were seen from first epoch up to the last epoch as

the building continued to go up. The DSM change will then be used to analyse how the building was changed in height throughout the construction period.
Though 1m thresholding gives at least good results compared to others, still the output suffers from noise (small isolated regions/pixels). Those small regions have to be cleaned up using the mathematical morphological operation opening. The remaining output is shown in Figure 12 were by some small regions where removed.

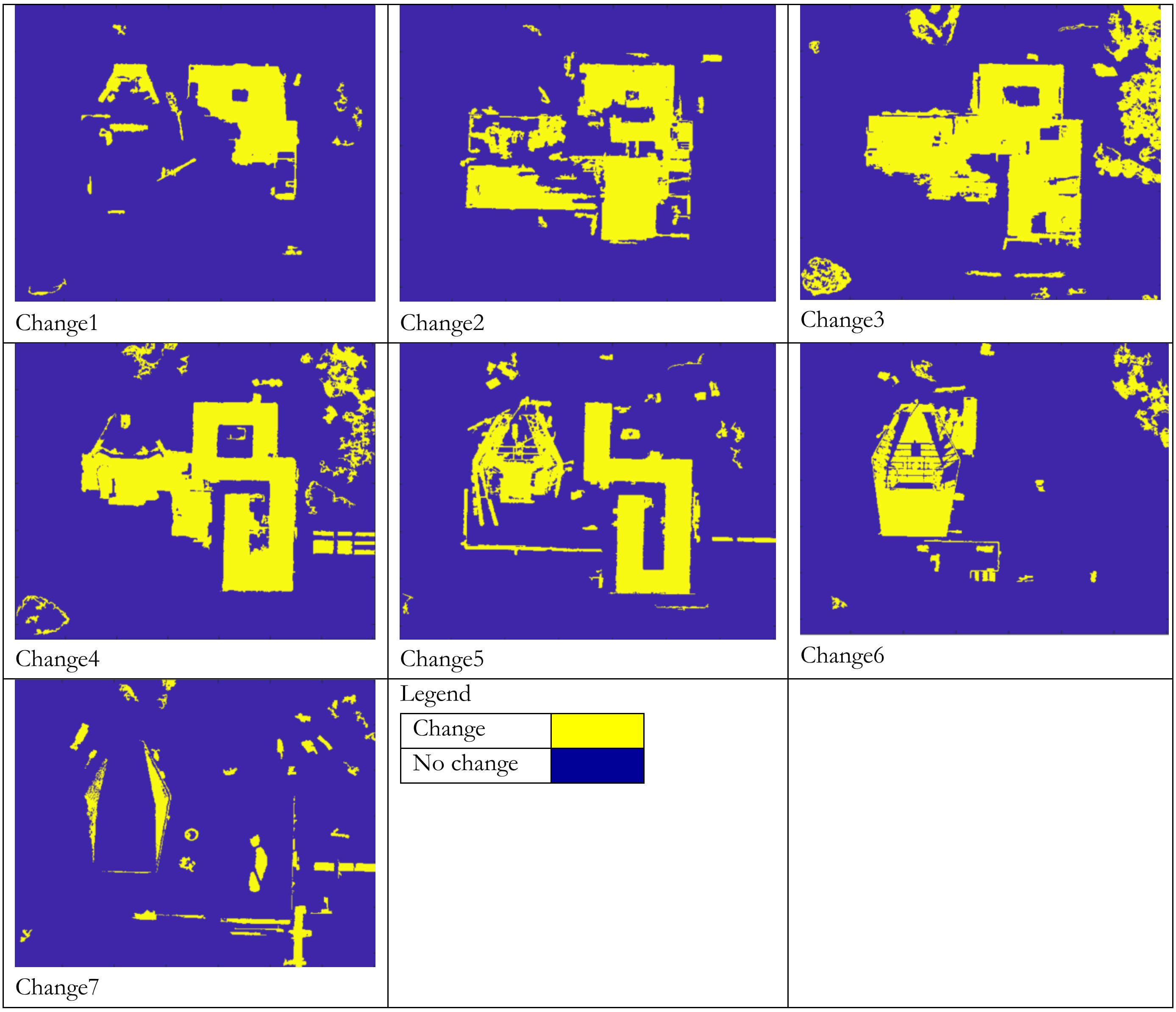

Figure 12: DSM changes

The accuracy assessment for the new clean up DSM change was conducted as it is shown in Table 3 which gives more accurate results.

Table 3: Overall accuracy of the DSM change with removal of noise

Change	Change1	Change2	Change3	Change4	Change5	Change6
Overall accuracy (%)	97.3	94.9	89.2	93.4	95.2	94.8

5.2. Post classification change detection

The following subsections will provide the results and analysis done for the post classification change detection method. Different experiments conducted including fully connected CRF parameter tuning, classification using 2D features only, classification using 2D and 3D features, change detection results and the improvement of the classification accuracy.

5.2.1. Fully connected CRF parameter tuning

From the fully connected CRF equation explained in section 2.3, there are three parameters which are weights, positional range and colour range. All these parameters were varied accordingly and found that on average when, $\theta_\gamma = 40$, and $\theta_\beta = 5$, gives more accurate results than the others as it can be shown in Table 4. The weight value varies, in epoch 5 and epoch 6 the $w = 0.1$ gives more accurate results and in epoch 7 and 8 $w = 0.5$ gives more accurate results. However when using $w = 0.1$ the visualization of the output become more smoothed and even some times it gives a false label to some pixels as it can be seen in Figure 13 which shows the output of classification for epoch five with different parameters. From the figure, when w=0.1 road was classified to bare soil which gives bad classification results. Due to that $w = 0.5$ was then selected to be the more suitable parameter for the classification of the given images.

Table 4: Fully connected CRF parameter tuning

w	θ_γ	θ_β	Epoch 5	Epoch 6	Epoch 7	Epoch 8
1	60	10	64.9	66.4	73.6	67.4
1	40	10	64.9	67.5	73.5	69.4
1	40	5	65.9	68.4	75.4	71.8
0.7	40	5	65.9	69.6	75.6	72.1
0.5	**40**	**5**	**66.3**	**70.5**	**76.1**	**72.1**
0.1	40	5	66.8	71.5	75.5	70.7
0.1	20	5	66.5	71.2	73.2	70.0
0.1	10	5	66.6	70.9	72.8	70.0

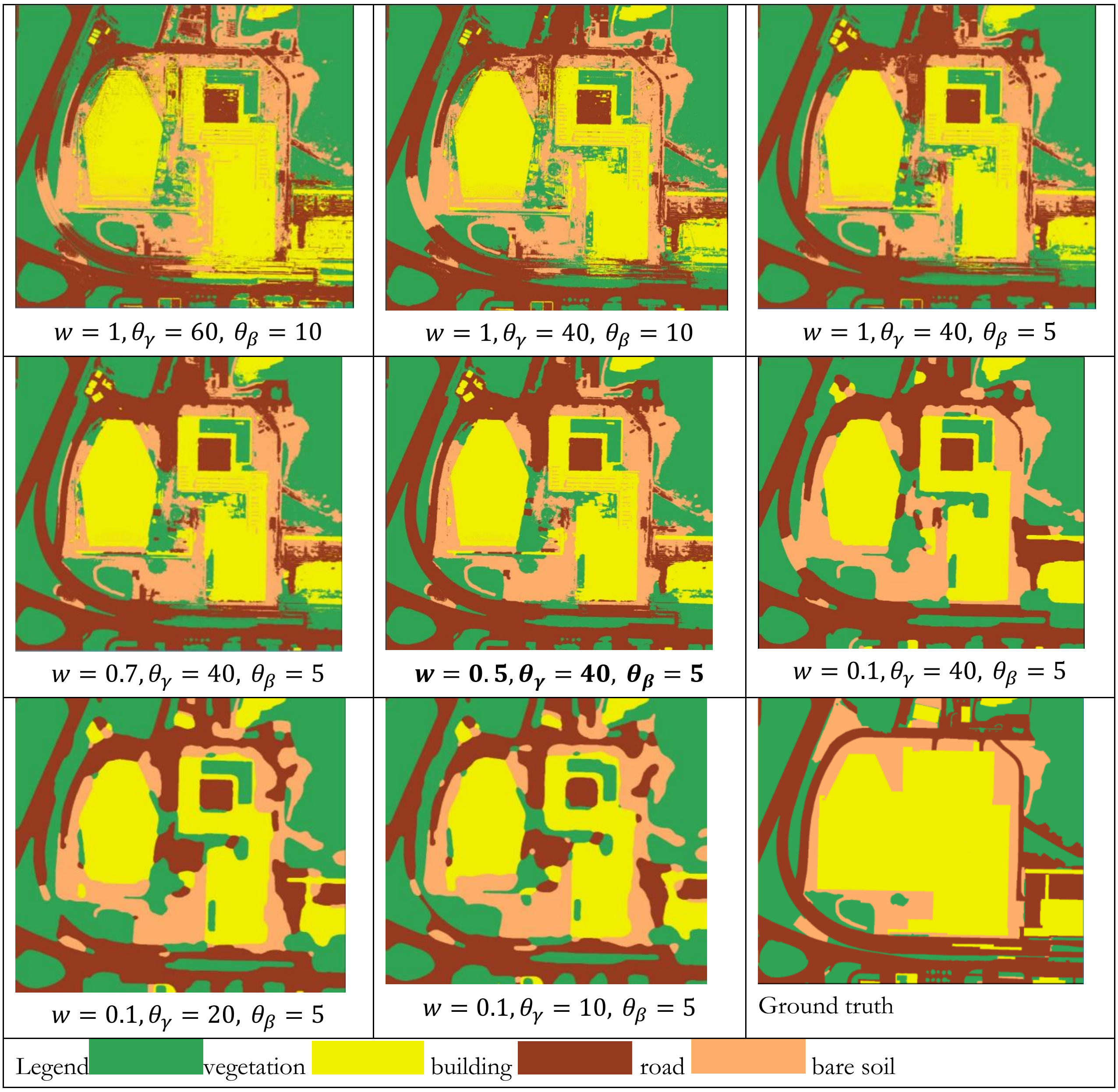

Figure 13: Classification results for epoch seven with different fully connected CRF parameters, highlighted parameters are the one with higher accuracy

5.2.2. 2D classification

Random forest classifier as the unary part of CRF is used whereby training was done using the first four epochs. The first experiment conducted using only 2D features for classification purpose. The feature extracted was HSV features and the GLCM features. After the training of the classification model, it was tested using epoch 5 to epoch 8.

The results from the random forest contain a lot of noise as it is shown in Figure 14. So fully connected CRF was then applied to smoothen the classification results. As it is explained in the section 4.3.2, after application of the fully connected CRF, the results were then refined, and small isolated labels was removed, and the boundary between one label and the other was defined clearly.

	Random Forest	FCCRF	GT
EPOCH 5	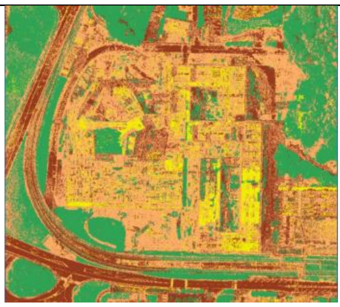	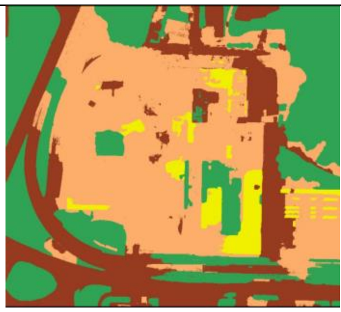	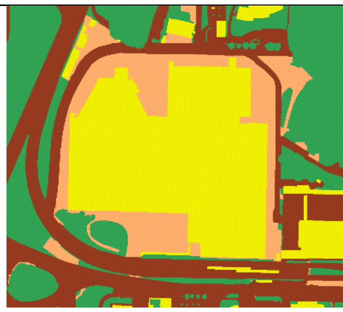
EPOCH 6	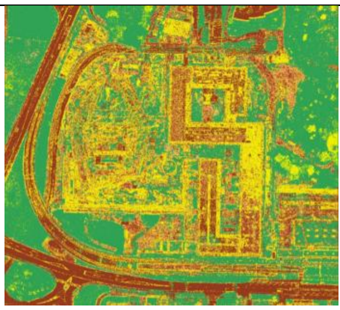	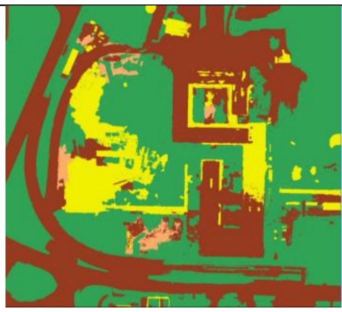	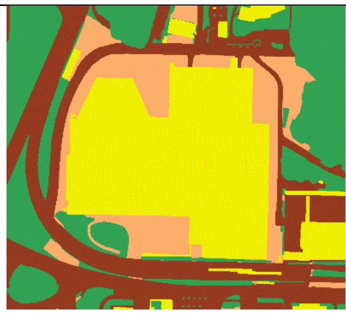
EPOCH 7	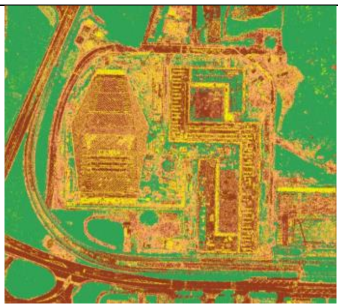	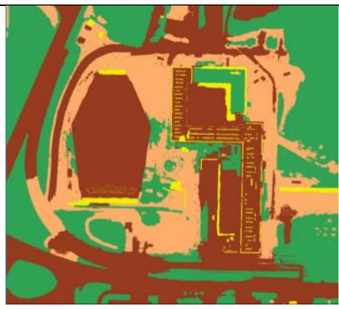	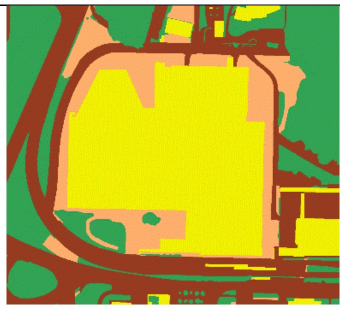
EPOCH 8	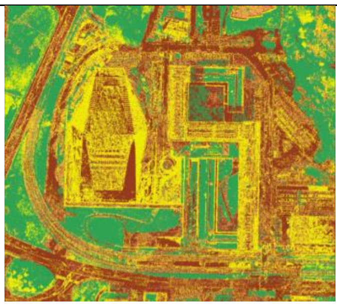		
Legend vegetation Building Road Bare soil			

Figure 14: 2D classification results

By using confusion matrix presented in Appendix C which was generated from the predicted labels and the reference data, the overall accuracy and IoU score for both random forest and fully connected CRF were computed. Table 5 shows the percentage accuracy for all the epochs.

Table 5: Accuracy assessment for 2D classification

	Random forest		FCCRF	
	OA (%)	IoU (%)	OA (%)	IoU (%)
Epoch 5	50.4	34.9	57.9	42.4
Epoch 6	52.5	33.1	56.7	33.6
Epoch 7	51.9	34.9	57.7	40.4
Epoch 8	50.6	31.7	57.7	40.4

5.2.3. 2D and 3D classification

Another experiment conducted using 2D features from the orthophoto, and geometric features from DSM was used for classification. The same 2D features were used for classification and the DSM features used was linearity, planarity and normalized DSM. Classification output for the remaining epochs gives better results compared to classification using 2D features alone. Figure 15 shows the results of the random forest, fully connected CRF and the respective ground truth.

	Random forest	Fully connected CRF	Ground truth
Epoch5	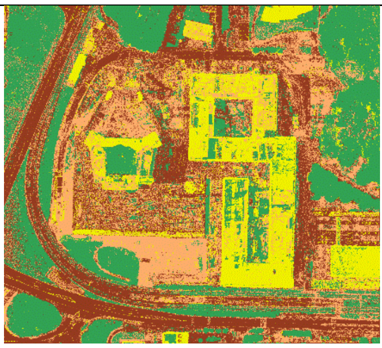		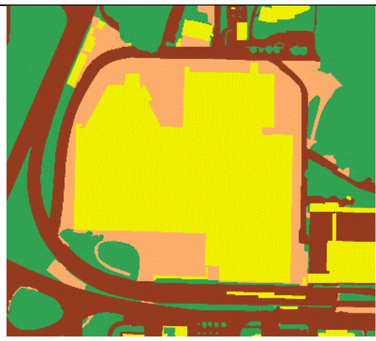
Epoch6	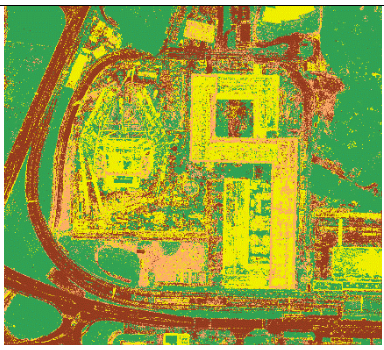	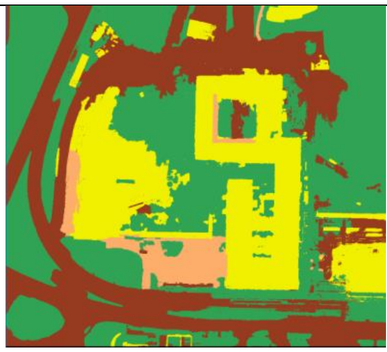	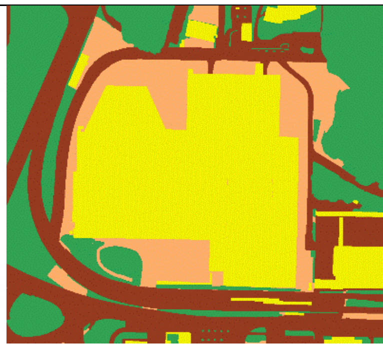
Epoch7	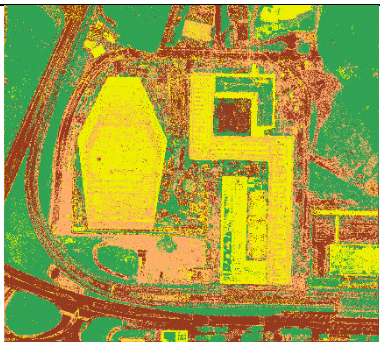	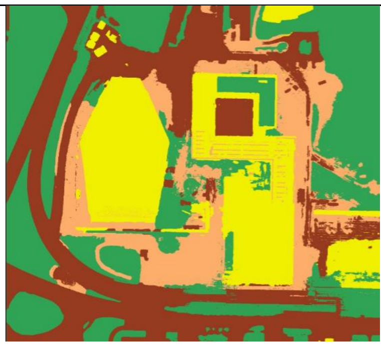	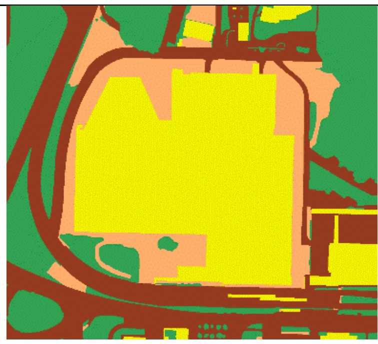

Epoch8	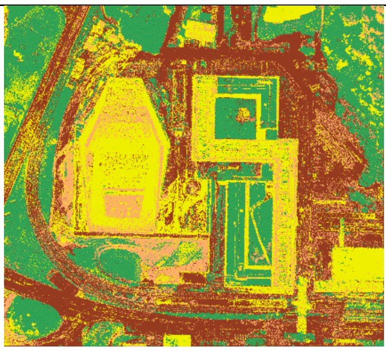	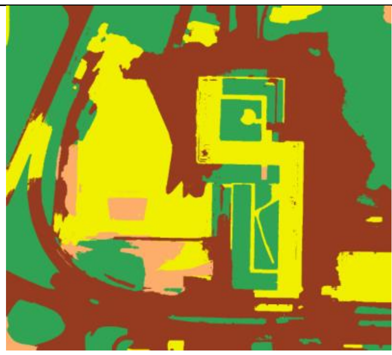	
Legend	vegetation	Building	Road Baresoil

Figure 15: 2D and DSM features classification results

Overall accuracy and IoU score were computed using confusion matrix in Appendix C. The visualization and accuracy of the result have improved compared to the accuracy of the 2D features classification. The accuracy assessment for the above experiment is presented in Table 6.

Table 6: Accuracy assessment for 2D and DSM classification

	Random forest		FCCRF	
	OA (%)	IoU (%)	OA (%)	IoU (%)
Epoch 5	59.7	42.2	66.3	47.6
Epoch 6	62.1	42.3	70.5	49.3
Epoch 7	63.1	45.1	76.1	59.6
Epoch 8	59.1	39.3	72.1	49.4

5.2.4. Change detection

Post classification change detection was applied, whereby two classified map from consecutive epochs were overlaid, and change between them was detected. From four classes, when overlying 16 classes are a possible outcome to be generated. But some of the generated classes are not relevant, example changing from building to bare soil, changing from road to bare soil which they are generated due to misclassification of some parts in those epochs. From the provided epochs, a lot of change appeared in the first three epochs than the rest of the epochs. Figure 16 shows the change detection for epoch 5 and 6, epoch 6 and 7, and epoch 7 and 8 with their respective change of the ground truth.

	Change map	GT change
Epoch 6-epoch 5	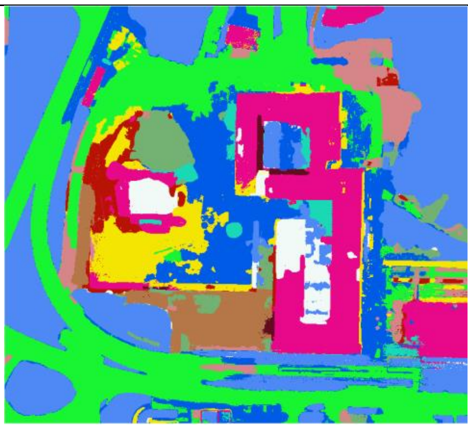	

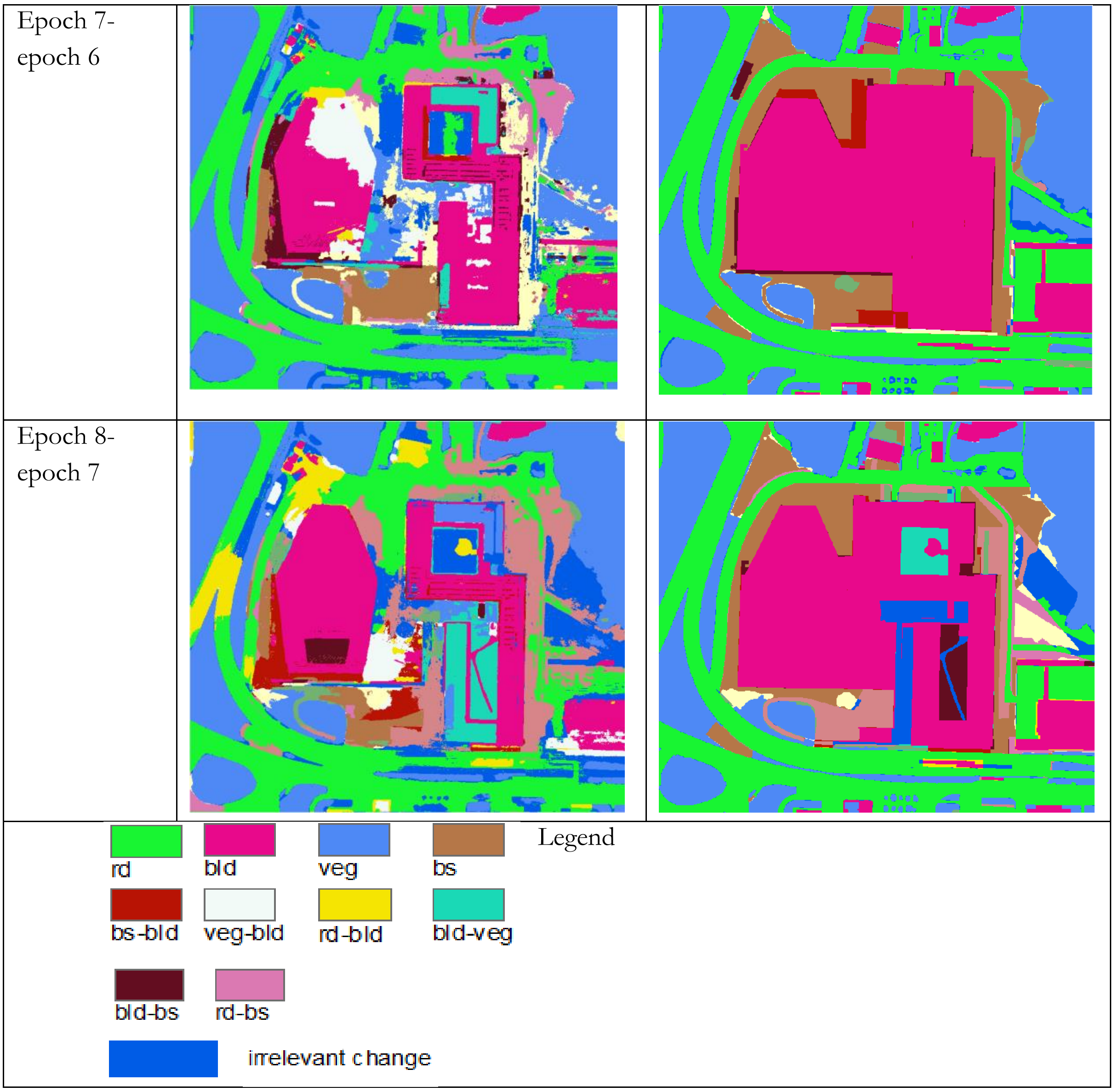

Figure 16: Change detection results with legend

Accuracy assessment for the change detection was done using overall accuracy. Confusion matrix for change detection accuracy assessment was generated using the predicted change map, and the ground truth change map (Appendix E) as it is presented in Appendix F. Table 7 shows the overall accuracy of the changes generated from the classified change map.

Table 7: Change detection accuracy

	OA (%)	IoU (%)
Change 1	58.0	13.5
Change 2	62.6	14.3
Change 3	60.5	19.0

5.2.5. Improving the results

Upon trying to improve change detection accuracy, another experiment was done with the addition of training samples from the classified epoch. Table 8 shows the number of training samples added for each epoch and the distribution for each class. Selection of the added samples considered the area which has worst classification result. By adding those samples, the accuracy of the classification increased by 1.6%.

Table 8: Number of samples added during the training of random forest

	Number of samples	Number of sample for each pixel
Epoch5	370800	Road=1217 Building=323281 Vegetation=1036 Bare soil=45266
Epoch6	241488	Road=5824 Building=187501 Vegetation=0 Bare soil=48163
Epoch7	216033	Road=1052 Building=182462 Vegetation=117 Bare soil=32402
Epoch8	286104	Road=55858 Building=177870 Vegetation=35973 Bare soil=16403

From the above training samples, new classification results were generated. Figure 17 and Table 9 shows the results for epoch 5 to epoch 8 and the accuracy assessment for the new results computed from confusion matrix in Appendix D respectively.

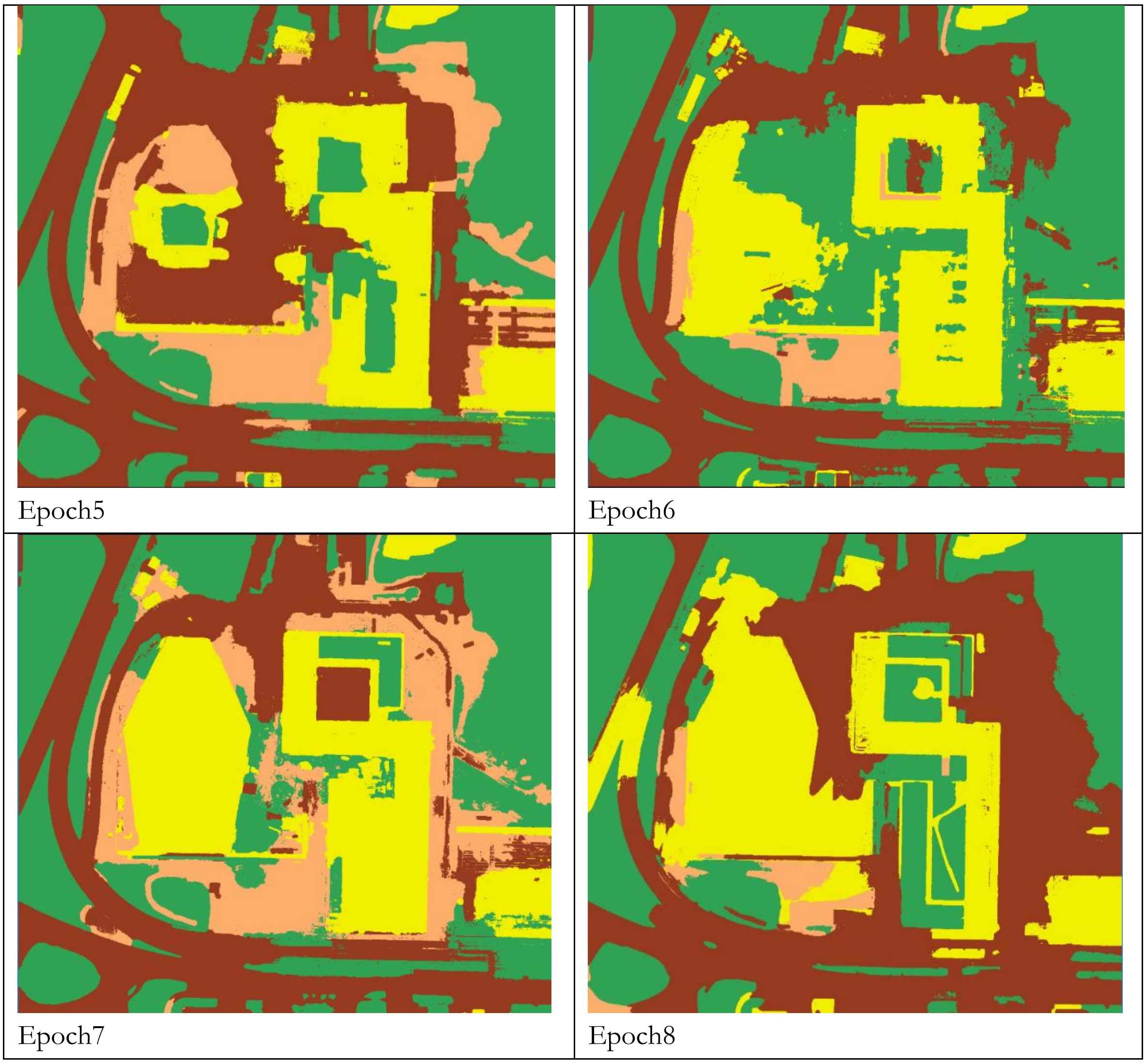

Figure 17: Improved classification results

Table 9: Accuracy assessment for the improved results

	Random forest		FCCRF	
	OA (%)	IoU (%)	OA (%)	IoU (%)
Epoch 5	60.6	43.0	67.9	49.5
Epoch 6	63.8	43.7	71.6	50.4
Epoch 7	64.6	46.6	77.2	61.3
Epoch 8	62.6	42.0	72.8	50.0

Adding the training samples during classification increases the overall accuracy of the change detection up to 1.8%. Due to the small amount of accuracy increased the visualization of the change detection map does not show big improvement. Figure 18 shows the change detection map from the classified epochs with additional samples followed by Table 10 which shows the accuracy assessment for the change detection map generated from confusion matrix in Appendix G.

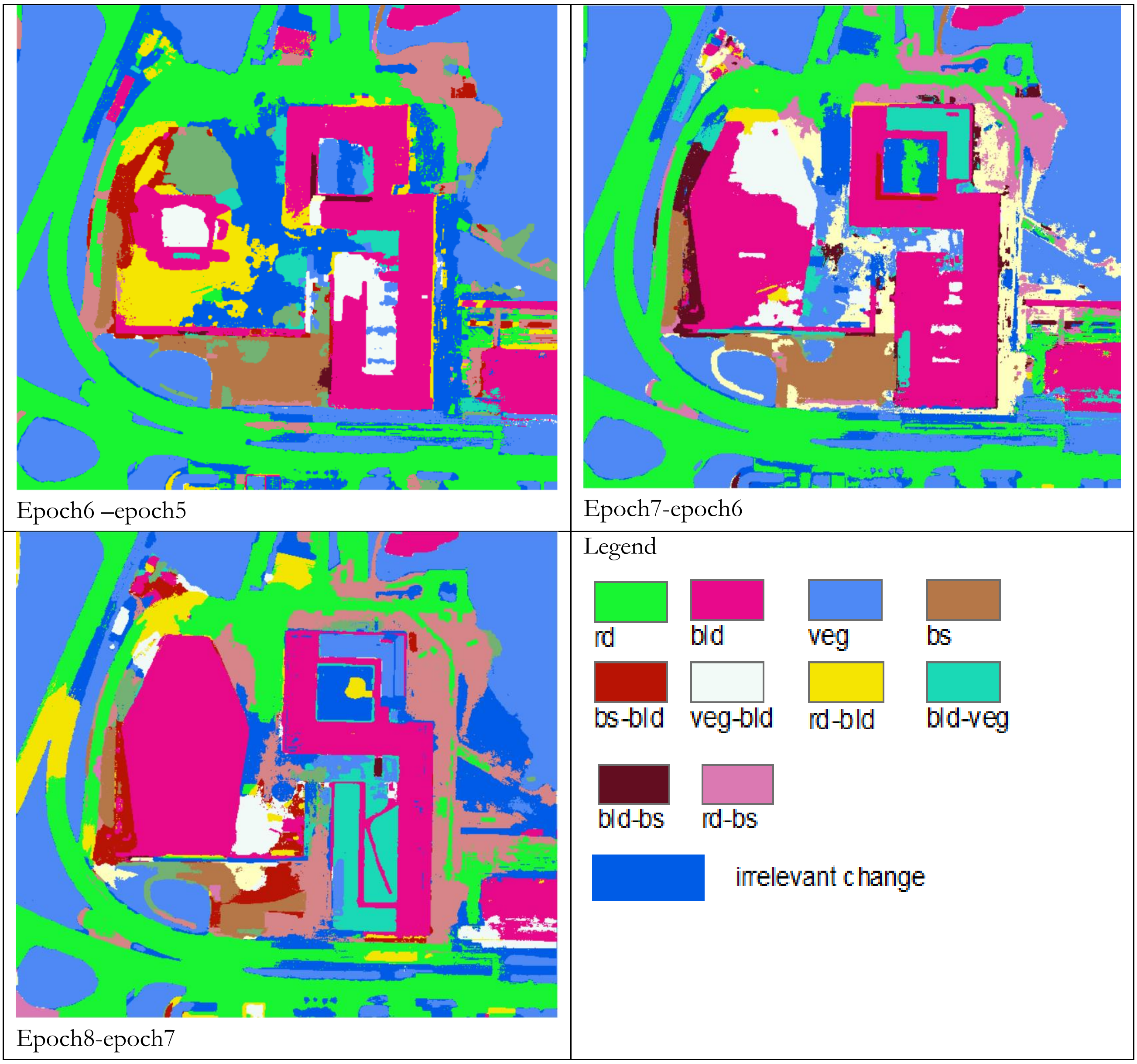

Figure 18: Improved change detection results

Table 10: Improved change detection accuracy

	OA (%)	IoU (%)
Change 1	59.8	13.9
Change 2	63.9	14.7
Change 3	62.0	19.4

By using the IoU score computation table presented in Appendix F and Appendix G, it was possible to determine the class changes that do not perform well which leads to the poor overall IoU score. These class changes are building-bare soil, road-bare soil, road-building, vegetation-building and building-road. These class changes have low IoU scores due to the misclassification as the post classification change detection depends much on the classification of the individual image.

5.3. Pre classification change detection

As it was done in the post classification change detection approach, here also the first four epochs was used for training, and the last four epochs were used for testing the classifier. Features were extracted in each epoch. The change of the features for training were calculated for epoch2-epoch1, epoch3-epoch2 and epoch4-epoch3. The random forest was used for training and classification of the changed features of the remaining four epochs. Fully connected CRF was applied for the refinement of the classification result from the random forest.

Two sets of experiments were done at this stage for testing how 2D and DSM features perform in classification. The first one uses all 2D and DSM features and the second approach used only 2D features for change detection followed by classification of those changes.

5.3.1. Using 2D and DSM features

In this part, the changes between the extracted features were detected first followed by the classification of the changes. The same features are used as in section 5.2.2. After feature extraction, changes between the features was detected followed by the classification of changes. The classification was done using random forest classifier followed by fully connected CRF for smoothening of the classification results. The first four epochs were used to train the random forest classifier, and the remaining four used for testing the model. The results for the classification of changes is as shown in Figure 19.

	Random forest	Fully connected CRF	Ground truth
Change 1	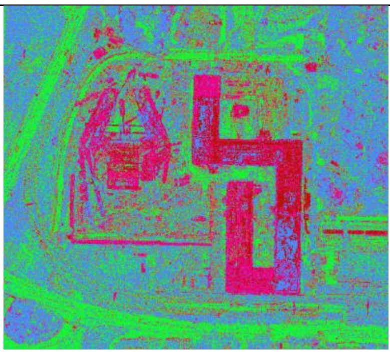	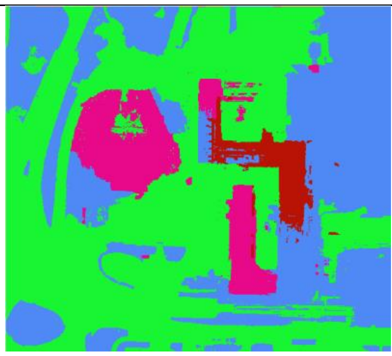	
Change 2	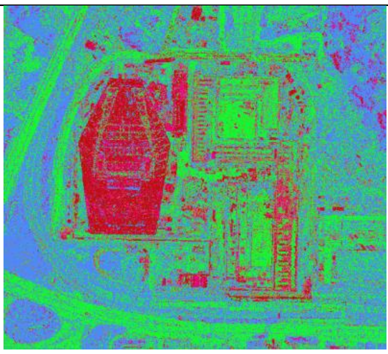		

Change 3	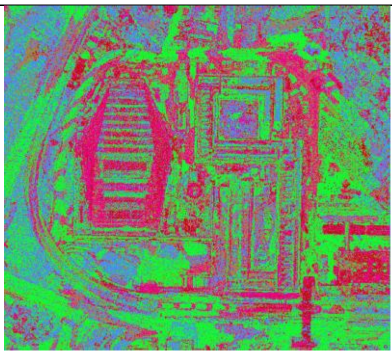		

Figure 19: Results of the classification of change using 2D and DSM features

The accuracy assessment from the generated confusion matrix in Appendix H was used to compute the overall accuracy and the IoU score shown in Table 11.

Table 11: Accuracy assessment for change classification

	Random forest		FCCRF	
	OA (%)	IoU (%)	OA (%)	IoU (%)
Change 1	32.6	5.0	41.3	5.3
Change 2	33.4	5.1	46.5	7.3
Change 3	23.7	3.8	39.7	7.1

5.3.2. Using 2D features

Classification of change features was also done using 2D features alone. HSV and GLCM features were extracted and used to find changes between the epochs. The changes were then classified using random forest followed by fully connected CRF to smoothen the results. Figure 20 shows the classification of changes whereby in this approach only a few classes were detected not like in the post classification change detection technique followed by Table 12 which shows the accuracy assessment in terms of overall accuracy and IoU score.

	Random forest	Fully connected CRF	Ground Truth
Change 1	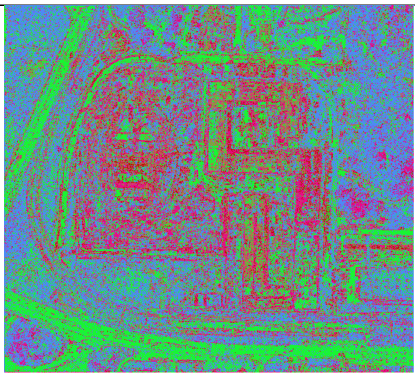		

Change 2	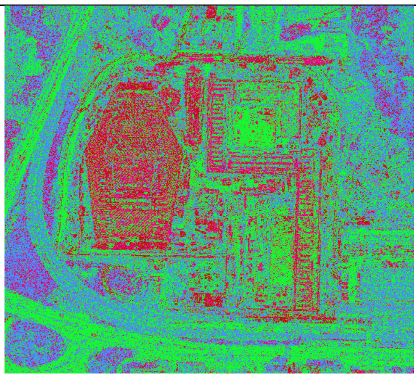		
Change 3	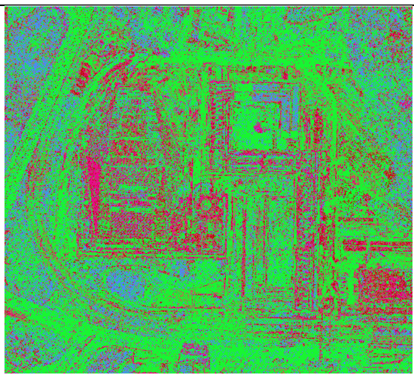	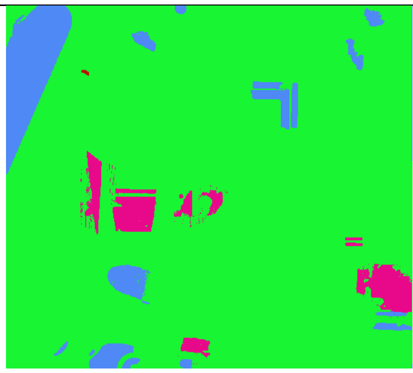	

Figure 20: Results for change classification using 2D features

Table 12: Change classification accuracy

	Random forest		FCCRF	
	OA (%)	IoU (%)	OA (%)	IoU (%)
Change 1	29.7	4.5	44.2	5.9
Change 2	29.9	4.4	41.8	6.4
Change 3	26.2	3.7	31.5	3.4

5.4. Integrating the DSM change and class change

This additional subsection will integrate the DSM change and class change for a better understanding of the change detection for the study area. For the construction area, most of the changes that take place are height changes which in our case can be observed using the DSM. The class change (like moving from bare soil to building and others) was expected to take place only in the first epochs of the dataset. And in this research, the first four epochs were used for training the classifier and using the last four epochs to test the performance of the classifier.

For the clear understanding of how changes takes place, DSM change and class change were combined. The change area from DSM was clipped, and a similar area in the class change was clipped for better understanding. In Figure 21 and Figure 22 for epoch6-epoch5 and epoch7-epoch6 changes respectively, it can be observed that there is a change in DSM while there is no class change which means that the building continued to be constructed from one floor to another with the same class (building).

Figure 21: Class change and DSM change for epoch 6 - epoch 5

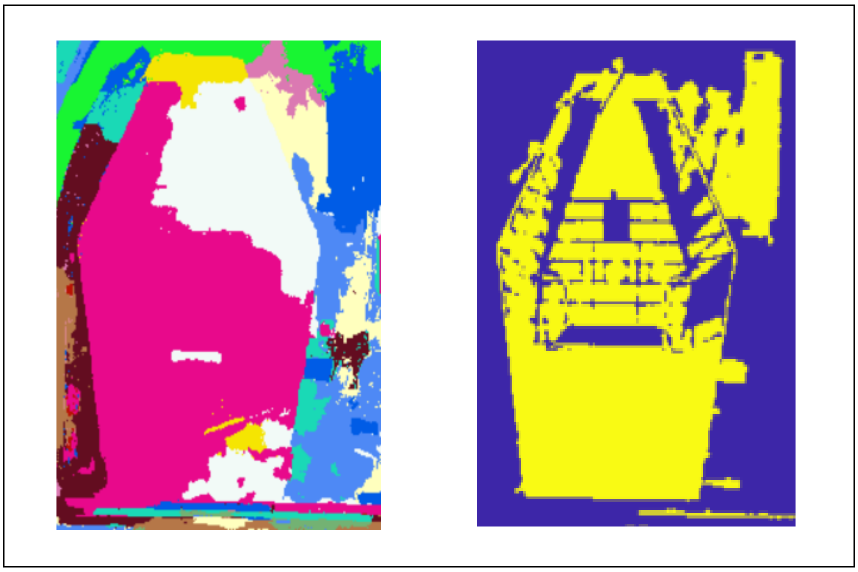

Figure 22: Class change and DSM change for epoch 7- epoch 6

In Figure 23 for epoch 8-epoch7 changes, there is no much DSM change because at that stage the construction activities were going to the last stages. Also in the features like road and vegetation can be observed that there was no class change as well as DSM change as it can be shown in the figure using a black circle. When observing the change between the first two epochs in Figure 24 where the class change generated from the ground truth and the DSM change from height differencing, it can be observed that there are some areas where there is height change with respect to class change (green circles) which means the area was changed from bare soil to building, and also the height changed. In the other way, there is another part of the area with a black circle where there is a change in class but it does not show height change, this means that the area was just starting to be constructed that it changes from bares soil to building with a small change of height.

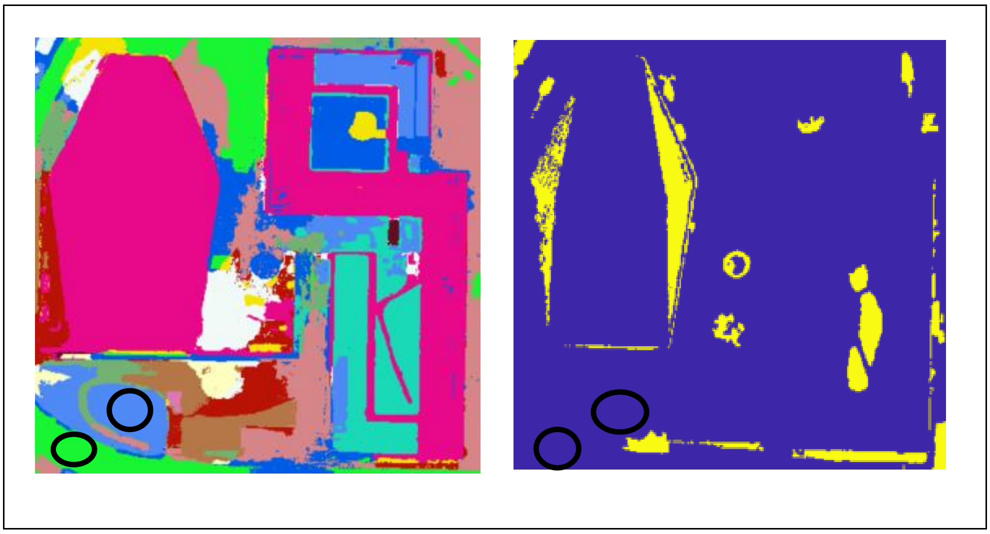

Figure 23: Class change and DSM change for epoch 8-epoch7

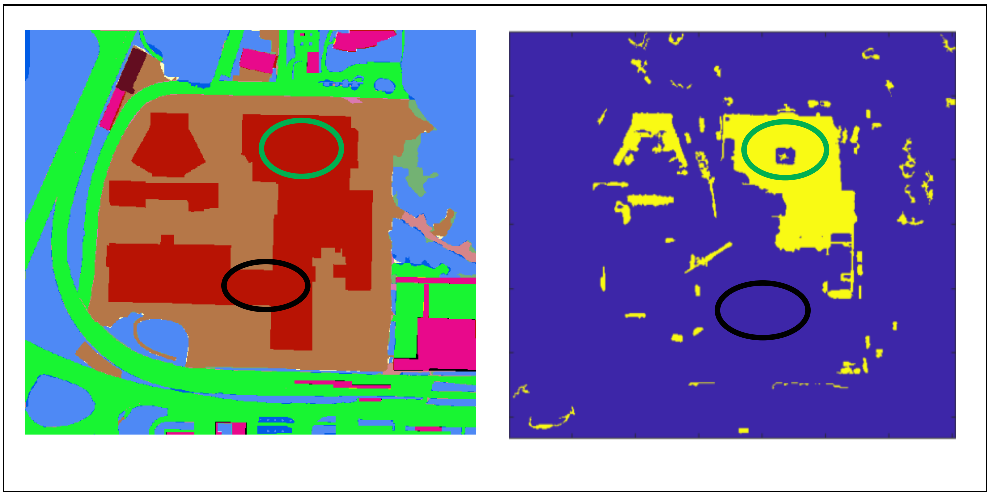

Figure 24: Class change and DSM change for epoch1-epoch 2

6. DISCUSSION

This research was focusing on applying the fully connected CRF for the classification and change detection of very high resolution UAV images. Very important aspects and output of the research will be discussed in this chapter. The aspects to be discussed include DSM change detection, feature importance, fully connected CRF parameter tuning, classification results and comparison of change detection methods applied in this study.

6.1. DSM change detection

On deciding the best thresholding value to be used for DSM change detection, 1m was found to have high accuracy than 0.3m and 0.5m. 0.3m and 0.5m do not give good results because in most cases at construction sites there are other activities which take place there like moving cars, construction tools which probably lie on that height values. However, DSM change from 1m thresholding value still suffers from noise which was removed using morphological operation opening results in a very high overall accuracy of up to 97.3%.

6.2. Feature importance

The features generated from the orthophoto and the features generated from the DSM was used in this study. On checking these feature importance, the classification was done in two different experiments. The first experiment was done using orthophoto features and the second experiment was done using orthophoto and DSM features. Adding the DSM features increases the classification accuracy up to 11% compared to the classification conducted using orthophoto features alone. The increase of accuracy shows the importance of integrating these features during classification process which have also been done by Gevaert et al. (2017)who uses 2D, 2.5D and 3D features and got high accuracy for informal settlement classification.

6.3. Fully connected CRF parameters

Three parameters from the fully connected CRF algorithm was tuned to find the best parameters which give higher accuracy than the others. The positional standard deviation which gives an average good result was 40, and the standard deviation for colour was 5. Also, the weight of the fully connected CRF was tuned and found that 0.5 gives average good accuracy compared to others. These standard deviations define the extent of the longer range. For classification of epoch 5 and epoch 6 it can be observed that when using the weight of 0.1 is where you get high accuracy, but again when comparing the results from the weight of 0.5 and 0.1, it can be observed that when using 0.1 the result is more smoothed and do not depict the reality. In Figure 25 when looking at the blue circle, it can be observed that when weight is 0.1 a part of the road was classified as the bare soil, means when continuing to reduce the weight value, the output will become more smoothed and far from the reality.

$w = 0.5, \theta_\gamma = 40,\ \theta_\beta = 5$ | $w = 0.1, \theta_\gamma = 40,\ \theta_\beta = 5$

Figure 25: Comparison of the classification results with w=0.5 and w=0.1

6.4. Classification results

Random forest output suffers from a lot of noise due to the absence of using neighbour information on defining the class label of the pixel. The application of fully connected CRF reduces the noise for the big extent which results in very smooth and clear boundary classified map. But still, the classifier fails to distinguish some of the areas due to the similarity in spectral properties. By using the IoU score which controls the classification accuracy for each class, it can be observed that the class with high IoU score was vegetation and with worst IoU score was bare soil. Class building and road have almost similar IoU score. All these scores presented in Table 13 whereby for each class the IoU was computed and followed by the overall IoU score for the whole image.

Table 13: IoU score for epoch 7 classification output

	Road	Building	Vegetation	Bare soil
TP	388183	364998	445555	161442
FP	103858	226173	10865	86663
FN	135627	12547	153416	125969
TN	1160069	1184019	1177901	1413663
IoU	**0.618453**	**0.604584**	**0.730614**	**0.431578**
IoU score		**0.596307**		

From the above table, it is observed that it was difficult to classify bare soil class due to some similarity in spectral properties with other classes like road and building. However, vegetation class was well classified in most of the epoch because it has different spectral properties compared to other classes.

Despite increasing the training samples from the classified epoch to improve the classification results, the accuracy increase only by 1% and there was no much improvement for the visualization of the classified epochs. This could be caused by the nature of the input images which seems to contain a lot of features with similar spectral properties.

6.5. Change detection comparison

From the two class change detection approaches that have been applied in this research, post classification change detection have seen to outperform the pre classification change detection method. The accuracy of the post classification change detection was 21% higher than the accuracy of the pre classification change detection. In addition to that, post classification allows detection of many changes (about 16 classes) but when using pre classification change detection only a few classes were able to be detected (about five classes). Post classification change detection results were not as good as it was supposed to be due to misclassification of the individual epoch. The features from the input images sometimes looked similar, especially for building, bare soil and road. The only feature which was clearly classified was vegetation. This leads to the poor presentation of the change detection map produced as it can be seen in Figure 26 for the change map of epoch 5 and epoch 6. Even after trying to improve the accuracy by adding more training samples but still, there was no visual improvement in change detection.

Figure 26: Change detection for epoch 6 and epoch 5

The importance of using DSM features have also been revealed in the pre classification change detection technique. Pre classification was conducted in two different experiment, whereby the first experiment use both 2D and DSM features and the second experiment uses 2D features alone. The accuracy assessment for both experiments was conducted and found that pre classification change detection using both 2D and DSM features alone outperform by 9% compared to pre classification change detection using 2D features alone.

Integrating the class change and DSM change gives a clear understanding of how the change takes place in an area. Most of the changes appeared in the DSM change than class change because the building was constructed upward from one floor to another. The class change takes place in the first stages of the construction. For visualization purpose, the DSM change and class change was cropped from their original results to have the good looking map.

7. CONCLUSION AND RECOMMENDATION

7.1. Conclusion

The main objective of this research was to propose a reliable approach for automatic classification and change detection within a scene using DSM and orthophoto generated from UAV images. A total of three change detection methods have been tested.

The first method was based on the DSM changes, whereby height information from one epoch was subtracted from height information of the next epoch. The output of this method was either there is a change or no change. The threshold value to distinguish between the change and no change was selected by visual inspection of the output and the accuracy assessment from the generated confusion matrix.

The last two methods use orthophoto and DSM features for change detection between the epochs. Post classification change detection and pre classification change detection was tested, and the performance was evaluated using accuracy assessment. These two approaches usefully connected CRF model for classification. Post classification outperforms pre classification change detection approach by 21% overall accuracy which leads us to the conclusion that post classification change detection method is superior to the pre classification change detection method.

DSM change and class change from post classification approach were then integrated to evaluate their relationship. For the case of building (construction area) change detection, it has been observed that class change is not enough to observe what has been changing, however combining these informations with DSM change as it can be seen in section 5.4 of this thesis, will give a good overview on what is going on in the construction area or even urban area.

The answers to the research questions that have been mentioned in Section 1.4 of this thesis are presented below.

1. What are the available algorithms for change detection?
   In Chapter 2, different change detection has been discussed. All those change detection methods based on two categories which are algebraic change detection and classification based change detection method.

2. What is the most suitable approaches to define the unary and pairwise potential terms in the CRF-model?
   In this study, we choose random forest to define the unary potential as it has been used by many studies as the robust classifier and does not take a lot of time during training. The pairwise potential was defined using fully connected CRF due to its ability to use all the information from the image to define the label of the single pixel

3. Which is the best change detection technique using a DSM as input?
   Since DSM contains only height information for each pixel in the image, the best way for change detection was using image differencing technique. By subtracting height information from one pixel of epoch 1 to the same pixel of epoch 2 a change image was generated. Thresholding was then used to define the changed and unchanged area. The noise from the DSM change was removed using the mathematical morphology opening.

4. How to use rule based to distinguish changed and unchanged DSM?
   Thresholding was used to distinguish between the change and unchanged DSM of the two epochs. Visual inspection was used to determine the best threshold to be used to distinguish between the change and unchanged part of the DSM result.

5. How to smooth the false changes due to DSM noise?
   From the DSM change detection, the false changes were smoothed using the mathematical morphology operation open which used to remove small regions that have been isolated from the DSM change detection output.

6. How to define the training for four classes?
   From the input orthophoto images, the main objects were road, railway, vegetation, bare soil, concrete and roof of the building. Among these objects, some of them have similar spectral properties (colour) including railway and road, concrete and roof of the building. So these similar features were combined and hence remaining with four classes which are road, building, vegetation and bare soil. From the eight epochs of data set, first for epochs was used during training of the classifier and the remaining was used to test the classification model. For the improvement of the classification accuracy, samples from the specific classified epoch was added during training and the accuracy increased by 1.6% compared to the classification results when only four epochs was used for training.

7. How to compose the pairwise potential for DSM and orthophoto?
   The pairwise potential for this research was composed using the fully connected CRF. Fully connected provides the long range connection on defining the label of the pixel which leads to the output with more accurate results. Despite getting more accuracy when using fully connected CRF but also it smoothens the classification output from the random forest classifier which was used to define the unary potential of the CRF.

8. What is the contribution of DSM and orthophoto in classification results?
   The contribution of DSM features can be seen during the classification. In section 5, classification results using orthophoto features and orthophoto with DSM features was presented separately. It was observed that when combining these features classification accuracy increase up to 18.2% compared to the classification using only orthophoto features.

9. What is the performance of the proposed algorithm using DSM and Orthophoto?
   The accuracy obtained from confusion matrix was used to evaluate the performance of methods used in this study. For the class change detection, post classification outperforms pre classification change detection. The overall accuracy of the post classification change detection was 62.6% while pre classification change detection was 46.5%.

10. How does fully connected CRF and random forest compared in terms of accuracy?
    Fully connected CRF plays a big role in smoothening classification results from the random forest. Random forest which gives the label to a pixel without considering the contextual information usually surfers from noise. Fully connected CRF is the used to smoothen and remove the noise as well as defining the boundary for each class clearly. This can also be observed when comparing overall accuracy of the fully connected CRF which is higher by 76.1% and of the random forest is 63.1% for one of the classified epoch. The increase of 13% shows that fully connected CRF is a very robust approach for classification of very high resolution images.

11. Can accuracy be improved by adding the training samples from the classified epoch?
    Addition of training sample from the specific classified epoch was expected to increase the accuracy and improving the classified map. However, the accuracy increase only by 1.6%, the small increase of accuracy did not improve the visualization of the classified map.

7.2. Recommendation

The ability of fully connected CRF in smoothening the results have been well shown in this study. Though it was difficult to separate some of the classes with similar spectral properties like bare soil, road and building in some epochs. Few recommendations have been given below.

- Further studies can be conducted to improve the accuracy of the classification of the very high resolution images like the one used in this study. This can be done by using different methodology apart from the one used.
- Since the big problem was classification of road, building and bare soil, different machine learning approach like CNN can be tested to check their ability in separating those classes which will result in very high accuracy.
- This study makes use of HSV, GLCM, linearity and planarity features, I suggest further study which will use different features for classification to test the performance of those features.
- The use of fully connected CRF for smoothening the DSM changes should further be investigated as it was not applied in this study.

LIST OF REFERENCES

Adam, E., Mutanga, O., Odindi, J., & Abdel-Rahman, E. M. (2014). Land-use/cover classification in a heterogeneous coastal landscape using RapidEye imagery: evaluating the performance of random forest and support vector machines classifiers. *International Journal of Remote Sensing*, *35*(10), 3440–3458. https://doi.org/10.1080/01431161.2014.903435

Afify, H. A. (2011). Evaluation of change detection techniques for monitoring land-cover changes: A case study in new Burg El-Arab area. *Alexandria Engineering Journal*, *50*(2), 187–195. https://doi.org/10.1016/j.aej.2011.06.001

Aicardi, I., Nex, F., Gerke, M., Lingua, A. M., Melgani, F., Martinsanz, G. P., … Thenkabail, P. S. (2016). An Image-Based Approach for the Co-Registration of Multi-Temporal UAV Image Datasets. *Remote Sensing Article*, *8*(779). https://doi.org/10.3390/rs8090779

Al Asmar, Y. Y., Koeva, M., & Gerke, M. (2017). VERY HIGH RESOLUTION OPTICAL SENSORS CAMERAS AND SATELLITE SYSTEMS, module 7 [PowerPoint slides]. Retrieved from https://blackboard.utwente.nl/bbcswebdav/pid-1008533-dt-content-rid-2426109_2/courses/U17-GFM-105/03_Very High Resolution Optical Sensors_2017.pdf

Argialas, D. P., Michailidou, S., & Tzotsos, A. (2013). Change detection of buildings in suburban areas from high resolution satellite data developed through object based image analysis. *Survey Review*, *45*(333), 441–450. https://doi.org/10.1179/1752270613y.0000000058

Bazi, Y., Bruzzone, L., & Melgani, F. (2005). An unsupervised approach based on the generalized Gaussian model to automatic change detection in multitemporal SAR images. *Geoscience and Remote Sensing, IEEE Transactions on*, *43*(4), 874–887. https://doi.org/10.1109/TGRS.2004.842441

Blomley, R., Weinmann, M., Leitloff, J., & Jutzi, B. (2014). SHAPE DISTRIBUTION FEATURES FOR POINT CLOUD ANALYSIS -A GEOMETRIC HISTOGRAM APPROACH ON MULTIPLE SCALES. *ISPRS*, *2*(3). https://doi.org/10.5194/isprsannals-II-3-9-2014

Bouziani, M., Goïta, K., & He, D.-C. (2010). Automatic change detection of buildings in urban environment from very high spatial resolution images using existing geodatabase and prior knowledge. *ISPRS Journal of Photogrammetry and Remote Sensing*, *65*, 143–153. https://doi.org/10.1016/j.isprsjprs.2009.10.002

Breiman, L. (2001). Random Forests. *Machine Learning*, *45*, 5–32. Retrieved from https://link.springer.com/content/pdf/10.1023%2FA%3A1010933404324.pdf

Campbell, J. B., & Wynne, R. H. (2011). *Introduction to remote sensing* (5th ed.). New York: Guilford Press. Retrieved from http://ezproxy.utwente.nl:2200/patron/FullRecord.aspx?p=843851

Cao, G., Zhou, L., & Li, Y. (2016). A new change-detection method in high-resolution remote sensing images based on a conditional random field model. *International Journal of Remote Sensing*, *37*(5), 1173–1189. https://doi.org/10.1080/01431161.2016.1148284

Chehata, N., Guo, L., & Mallet, C. (2009). AIRBORNE LIDAR FEATURE SELECTION FOR URBAN CLASSIFICATION USING RANDOM FORESTS, *38*(Paris, France). Retrieved from http://www.isprs.org/proceedings/XXXVIII/3-W8/papers/p207.pdf

Dalla Mura, M., Benediktsson, J. A., Waske, B., & Bruzzone, L. (2009). Morphological attribute filters for the analysis of very high resolution remote sensing images. *IEEE International Geoscience and Remote Sensing Symposium (IGARSS '09)*, *3*(10), 2–3. https://doi.org/10.1109/IGARSS.2009.5418096

Davis, J., & Goadrich, M. (2006). The relationship between Precision-Recall and ROC curves. In *Proceedings of the 23rd international conference on Machine learning - ICML '06* (pp. 233–240). New York, New York, USA: ACM Press. https://doi.org/10.1145/1143844.1143874

Dinand, A., Wietske, B., Ali, S., Zoltan, V., & Wouter, V. (2013). Data Integration. *The Core of GIScience*, 373–426. https://doi.org/10.1016/B978-0-12-385889-4.00013-2

El-Hattab, M. M. (2016). Applying post classification change detection technique to monitor an Egyptian coastal zone (Abu Qir Bay). *The Egyptian Journal of Remote Sensing and Space Science*, *19*, 23–36. https://doi.org/10.1016/j.ejrs.2016.02.002

Fan, H. (2013). Land-cover mapping in the Nujiang Grand Canyon: integrating spectral, textural, and topographic data in a random forest classifier. *International Journal of Remote Sensing*, *34*(21), 7545–7567. https://doi.org/10.1080/01431161.2013.820366

Feng, Q., Liu, J., & Gong, J. (2015). UAV Remote Sensing for Urban Vegetation Mapping Using Random Forest and Texture Analysis. *Remote Sensing*, *7*(1), 1074–1094. https://doi.org/10.3390/rs70101074

Frauman E, & Wolff E. (2006). CHANGE DETECTION IN URBAN AREAS USING VERY HIGH SPATIAL RESOLUTION SATELLITE IMAGES: CASE STUDY IN BRUSSELS, 2–3. Retrieved from http://citeseerx.ist.psu.edu/viewdoc/download;jsessionid=CDCD257F095F2F4B9299BE465D101090?doi=10.1.1.88.779&rep=rep1&type=pdf

Gevaert, C. M., Persello, C., Sliuzas, R., & Vosselman, G. (2017). Informal settlement classification using point-cloud and image-based features from UAV data. *ISPRS Journal of Photogrammetry and Remote Sensing*, *125*, 225–236. https://doi.org/10.1016/j.isprsjprs.2017.01.017

Ghosh, A., Mishra, N. S., & Ghosh, S. (2011). Fuzzy clustering algorithms for unsupervised change detection in remote sensing images. *Information Sciences*, *181*, 699–715. https://doi.org/10.1016/j.ins.2010.10.016

Hamuda, E., Mc Ginley, B., Glavin, M., & Jones, E. (2017). Automatic crop detection under field conditions using the HSV colour space and morphological operations. *Omputers and Electronic in Agriculture*, *133*, 97–107. https://doi.org/10.1016/j.compag.2016.11.021

Haralick, R., Shanmugan, K., & Distein, I. (1973). Textural Features for Image Classification. *IEEE Transactions on Systems, Man and Cybernetics*, *SMC-3*, *No. 6*(U.S.A), 610–621. Retrieved from http://haralick.org/journals/TexturalFeatures.pdf

Hong, F., Jianqing, Z., Zuxun, Z., & Zhifang, L. (1999). House change detection based on dsm of aerial image in urban area. *Geo-Spatial Information Science*, *2*(1), 68–72. https://doi.org/10.1007/BF02826721

İlsever, M., & Ünsalan, C. (2012). Pixel-Based Change Detection Methods. *Springer*, *10*, 7–22. https://doi.org/10.1007/978-1-4471-4255-3

Karantzalos, K. (2015). Recent Advances on 2D and 3D Change Detection in Urban Environments from Remote Sensing Data, *13*, 237–272. https://doi.org/10.1007/978-3-319-11469-9_10

Krähen, P., & Koltun, V. (2011). Efficient Inference in Fully Connected CRFs with Gaussian Edge Potentials. Retrieved from http://papers.nips.cc/paper/4296-efficient-inference-in-fully-connected-crfs-with-gaussian-edge-potentials.pdf

Leichtle, T., Geiß, C., Lakes, T., & Taubenböck, H. (2017). Class imbalance in unsupervised change detection – A diagnostic analysis from urban remote sensing. *Int J Appl Earth Obs Geoinformation*, *60*, 83–98. https://doi.org/10.1016/j.jag.2017.04.002

Leichtle, T., Geiß, C., Wurm, M., Lakes, T., & Taubenböck, H. (2017). Unsupervised change detection in VHR remote sensing imagery – an object-based clustering approach in a dynamic urban environment. *International Journal of Applied Earth Observation and Geoinformation*, *54*, 15–27. https://doi.org/10.1016/J.JAG.2016.08.010

Li, W., & Yang, M. Y. (2016). EFFICIENT SEMANTIC SEGMENTATION OF MAN-MADE SCENES USING FULLY-CONNECTED CONDITIONAL RANDOM FIELD. *International Archives of the Photogrammetry, Remote Sensing and Spatial Information Sciences - ISPRS Archives*, *23*. https://doi.org/10.5194/isprsarchives-XLI-B3-633-2016

Liu, H., & Zhou, Q. (2010). Accuracy analysis of remote sensing change detection by rule-based rationality evaluation with post-classification comparison. *International Journal of Remote Sensing*, *25*(5), 1037–1050. https://doi.org/10.1080/0143116031000150004

Liu, J., Feng, Q., Gong, J., Zhou, J., & Li, Y. (2016). Land-cover classification of the Yellow River Delta wetland based on multiple end-member spectral mixture analysis and a Random Forest classifier. *International Journal of Remote Sensing*, *37*(8), 1845–1867. https://doi.org/10.1080/01431161.2016.1165888

Liu, Z., Zhang, J., Zhang, Z., & Fan, H. (2003). Change Detection Based on DSM and Image Features in Urban Areas. *Geo-Spatial Information Science*, *6*(2), 35–41. Retrieved from https://ezproxy.utwente.nl:3351/content/pdf/10.1007%2FBF02826752.pdf

Lu, D., Mausel, P., Brondízio, E., & Moran, E. (2004). Change detection techniques. *International Journal of Remote Sensing*, *25*(12), 2365–2407. https://doi.org/10.1080/0143116031000139863

Marin-Jimenez, M. J., Zisserman, A., Eichner, M., Ferrari, · V, & Ferrari, V. (2013). Detecting People Looking at Each Other in Videos. *Springer Science*. https://doi.org/10.1007/s11263-013-0655-7

Mohanaiah, P., Sathyanarayana, P., & Gurukumar, L. (2013). Image Texture Feature Extraction Using GLCM Approach. *International Journal of Scientific and Research Publications*, *3*(1), 2250–3153. Retrieved from www.ijsrp.org

Na, X., Zhang, S., Li, X., Yu, H., & Liu, C. (2010). Improve Land Cover Mapping using Random Forests Combined with Landsat Thematic Mapper Imagerry and Ancillary Geographic Data. *Photogrammetric Engineering & Remote Sensing*, *76*(7), 833–840. Retrieved from

http://www.ingentaconnect.com/content/asprs/pers/2010/00000076/00000007/art00004?crawler=true
Nex, F., & Remondino, F. (2013). UAV for 3D mapping applications: a review. *Springer*. https://doi.org/10.1007/s12518-013-0120-x
Okenwa, A. I. (2016). *Change detection by the combination of 2D maps and height data*. University of Twente: Faculty of Geo-information Science and Earth Observation. Retrieved from https://ezproxy.utwente.nl:2315/library/2016/msc/gfm/okenwa.pdf
Otukei, J. R., & Blaschke, T. (2010). Land cover change assessment using decision trees, support vector machines and maximum likelihood classification algorithms. *International Journal of Applied Earth Observation and Geoinformation*, *12*, S27–S31. https://doi.org/10.1016/J.JAG.2009.11.002
Pal, M., & Mather, P. M. (2005). Support vector machines for classification in remote sensing. *International Journal of Remote Sensing*, *26*(5), 1007–1011. https://doi.org/10.1080/01431160512331314083
Peiman, R. (2011). Pre-classification and post-classification change-detection techniques to monitor land-cover and land-use change using multi-temporal Landsat imagery: A case study on Pisa Province in Italy. *International Journal of Remote Sensing*, *32*(15), 4365–4381. https://doi.org/10.1080/01431161.2010.486806
Persello, C. (2017). BASICS OF IMAGE PROCESSING. Retrieved from https://blackboard.utwente.nl/bbcswebdav/pid-1008543-dt-content-rid-2458052_2/courses/U17-GFM-105/GFM2_M8_2017_BIP.pdf
Qin, R. (2014). An Object-Based Hierarchical Method for Change Detection Using Unmanned Aerial Vehicle Images. *Remote Sensing*, *6*(9), 7911–7932. https://doi.org/10.3390/rs6097911
Sarp, G., Erener, A., Duzgun, S., & Sahin, K. (2014). An approach for detection of buildings and changes in buildings using orthophotos and point clouds: A case study of van erci?? earthquake. *European Journal of Remote Sensing*, *47*(1), 627–642. https://doi.org/10.5721/EuJRS20144735
Sesnie, S. E., Finegan, B., & Gessler, P. E. (2010). The multispectral separability of Costa Rican rainforest types with support vector machines and Random Forest decision trees. *International Journal of Remote Sensing*, *31*(11), 2885–2906. https://doi.org/10.1080/01431160903140803
Stow, D. A., Collins, D., & McKinsey, D. (1990). Land use change detection based on multi-date imagery from different satellite sensor systems. *Geocarto International*, *5*(3), 3–12. https://doi.org/10.1080/10106049009354263
Sun, X., Lin, X., Shen, S., & Hu, Z. (2017). High-Resolution Remote Sensing Data Classification over Urban Areas Using Random Forest Ensemble and Fully Connected Conditional Random Field. *ISPRS International Journal of Geo-Information*, *6*(8), 245. https://doi.org/10.3390/ijgi6080245
Théau, J. (2012). Change Detection. *Springer Handbook of Geographic Information*, *1*, 75–94.
Thomas Laidley. (2016). The Problem of Urban Sprawl - Contexts. Retrieved June 11, 2017, from https://contexts.org/articles/the-problem-of-urban-sprawl/
Unger, J., Reich, M., & Heipke, C. (2014). UAV-based photogrammetry: Monitoring of a building zone. *International Archives of the Photogrammetry, Remote Sensing and Spatial Information Sciences - ISPRS Archives*, *40*(5), 601–606. https://doi.org/10.5194/isprsarchives-XL-5-601-2014
Verikas, A., Gelzinis, A., & Bacauskiene, M. (2011). Mining data with random forests: A survey and results of new tests. *Pattern Recognition*, *44*, 330–349. https://doi.org/10.1016/j.patcog.2010.08.011
W, D. M. (2011). EVALUATION: FROM PRECISION, RECALL AND F-MEASURE TO ROC, INFORMEDNESS, MARKEDNESS & CORRELATION. *Journal of Machine Learning Technologies*, *2*(1), 37–63. Retrieved from http://dspace.flinders.edu.au/dspace/
Wu, C., Du, B., Cui, X., & Zhang, L. (2017). A post-classification change detection method based on iterative slow feature analysis and Bayesian soft fusion. *Remote Sensing of Environment*, *199*, 241–255. https://doi.org/10.1016/j.rse.2017.07.009
Wu, Q. ., Lu, Z., & Ji, T. (2009). Mathematical Morphology. *Springer*, *22*. https://doi.org/10.1002/9781118600788
Wu, S., Chen, H., Zhao, Z., Long, H., & Song, C. (2015). An improved remote sensing image classification based on K-means using HSV color feature. In *Proceedings - 2014 10th International Conference on Computational Intelligence and Security, CIS 2014* (pp. 201–204). https://doi.org/10.1109/CIS.2014.90
Xu, S., Vosselman, G., & Oude Elberink, S. (2015). DETECTION AND CLASSIFICATION OF CHANGES IN BUILDINGS FROM AIRBORNE LASER SCANNING DATA. *Remote Sensing*, *II-5*, 343–348. https://doi.org/10.5194/isprsannals-II-5-W2-343-2013
Xuan, W. (2011). Topographical Change Detection from UAV Imagery Using M-DSM Method, *228*, 596–605. Retrieved from http://link.springer.com/10.1007/978-3-642-23223-7_77

Yang, M. Y., & Förstner, W. (2011a). A Hierarchical Conditional Random Field Model for Labeling and Classifying Images of Man-made Scenes. *Remote Sensing of Environment*. Retrieved from https://blackboard.utwente.nl/bbcswebdav/pid-1059926-dt-content-rid-2617741_2/courses/M17-EOS-105/yang_2011_cvrs_hcrf.pdf

Yang, M. Y., & Förstner, W. (2011b). Regionwise classification of building facade images, *6952 LNCS*, 209–220. https://doi.org/10.1007/978-3-642-24393-6_18

Yousif, O., & Ban, Y. (2017). A novel approach for object-based change image generation using multitemporal high-resolution SAR images. *International Journal of Remote Sensing*, *38*(7), 1765–1787. https://doi.org/10.1080/01431161.2016.1217442

Zhou, L., Cao, G., Li, Y., & Shang, Y. (2016). Change Detection Based on Conditional Random Field with Region Connection Constraints in High-Resolution Remote Sensing Images. *IEEE Journal of Selected Topics in Applied Earth Observations and Remote Sensing*, *9*(8), 3478–3488. https://doi.org/10.1109/JSTARS.2016.2514610

APPENDICES

Appendix A: DSM change detection output with different thresholding

	0.3m	0.5m	1m	Smoothed change detection output
Change1	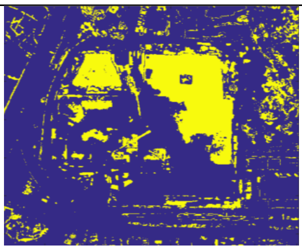	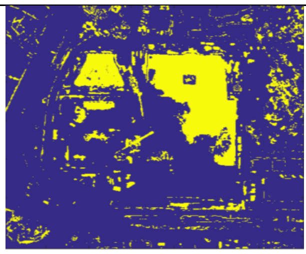	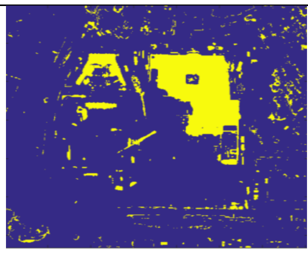	
Change2	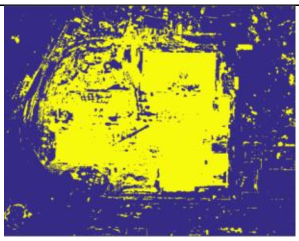	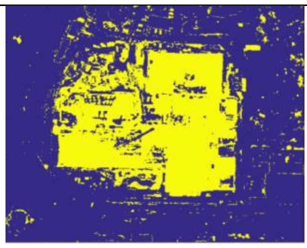	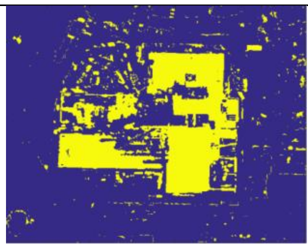	
Change3	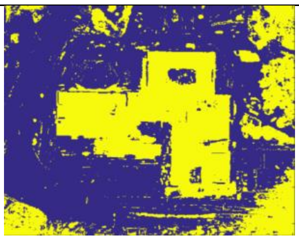		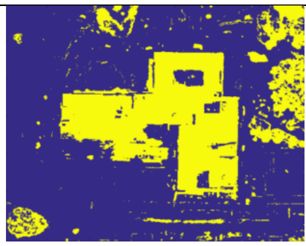	
Change4	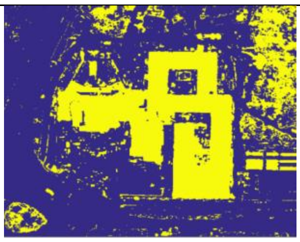	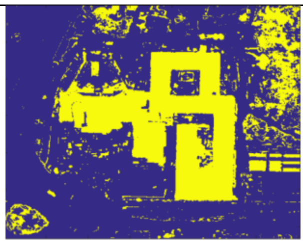	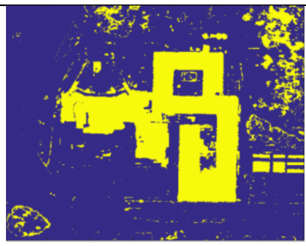	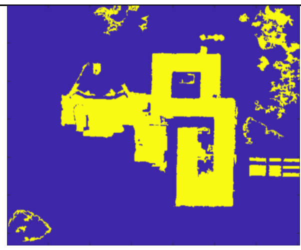
Change5				

Change6	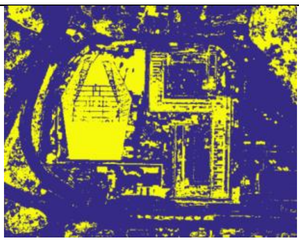	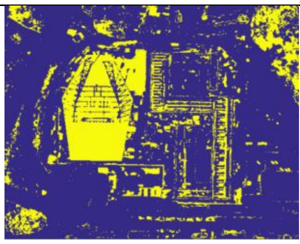	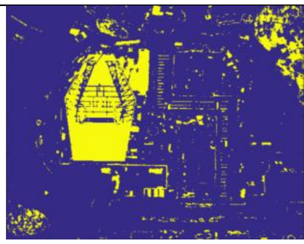	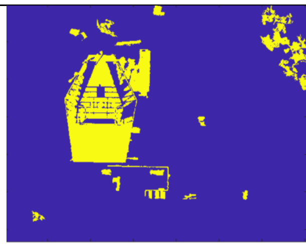

Legend

Change	
No change	

Appendix B: Confusion matrix for DSM change detection for the results of threshold=1m and the smoothed results

		threshold = 1m			smoothed results accuracy		
		No change	change		No change	change	
change1	No change	1565712	11377		1614996	11974	
	change	86287	124361	**94.5%**	37003	123764	**97.3%**
change2	No change	1413335	18764		1463597	18959	
	change	122254	233384	**92.1%**	71992	233189	**94.9%**
change3	No change	1213530	61781		1239365	63629	
	change	155558	356868	**87.8%**	129723	355020	**89.2%**
change4	No change	1338694	12744		1371896	12938	
	change	137880	297008	**91.6%**	104678	296814	**93.4%**
change5	No change	1413388	22835		1468177	23047	
	change	117444	232659	**92.1%**	62655	232447	**95.2%**
change6	No change	1501959	31053		1556983	37906	
	change	110348	144377	**92.1%**	55324	137524	**94.8%**

Appendix C: Confusion Matrix for the Fully Connected CRF for epoch 5 to 8 and their IoU scores computation table

Epoch 5 confusion matrix

Reference / Predicted	road	building	vegetation	bare soil
road	382583	4121	34397	59915
building	180035	254089	79041	66915
vegetation	14022	396	450095	8673
Bare soil	141856	2083	11013	97092
			Overall accuracy	**66.3%**

IoU computation table

	road	building	vegetation	Bare soil
TP	382583	254089	450095	97092
FP	98433	325991	23091	154952
FN	335913	6600	124451	135503
TN	969397	1199646	1188689	1398779
IoU	**0.468319**	**0.433096**	**0.753124**	**0.25053**
IoU score		**47.6%**		

Epoch 6 confusion matrix

Reference / Predicted	road	building	vegetation	bare soil
road	382137	13226	90923	2239
building	29433	374972	157054	21756
vegetation	7627	367	452086	104
Bare soil	101888	19119	83555	51251
			Overall accuracy	**70.5%**

IoU computation table

	road	building	vegetation	Bare soil
TP	382137	374972	452086	51251
FP	106388	208243	8098	204562
FN	138948	32712	331532	24099
TN	1160264	1171810	996021	1507825
IoU	**0.609009**	**0.608793**	**0.57102**	**0.183097**
IoU score		**49.3%**		

Epoch7 confusion matrix

Reference / Predicted	road	building	vegetation	bare soil
road	388183	6334	51898	45626
building	69577	364998	80715	75881
vegetation	6120	283	445555	4462
Bare soil	59930	5930	20803	161442
Overall accuracy				**76.1%**

IoU computation table

	road	building	vegetation	Bare soil
TP	388183	364998	445555	161442
FP	103858	226173	10865	86663
FN	135627	12547	153416	125969
TN	1160069	1184019	1177901	1413663
IoU	**0.618453**	**0.604584**	**0.730614**	**0.431578**
IoU score		**59.6%**		

Epoch8 confusion matrix

Reference / Predicted	road	building	vegetation	bare soil
road	489643	51311	44839	25278
building	77785	353762	54004	16834
vegetation	30878	5782	423451	3157
Bare soil	131173	32625	25287	20661
Overall accuracy				**72.1%**

IoU computation table

	road	building	vegetation	Bare soil
TP	489643	353762	423451	20661
FP	121428	148623	39817	189085
FN	239836	89718	124130	45269
TN	935563	1194367	1199072	1531455
IoU	**0.575437**	**0.597467**	**0.720893**	**0.081019**
		49.4%		

Appendix D: Confusion Matrix for the Fully Connected CRF for epoch 5 to 8 with additional of more samplesand their IoU scores computation table

Epoch 5

	road	building	vegetation	Bare soil
Road	378694	4759	34327	63236
Building	161185	287703	70436	60756
Vegetation	13639	413	450276	8858
Bare soil	141903	2110	11051	96980
			Overall accuracy	**67.9%**

IoU computation table

	road	building	vegetation	bare soil
TP	378694	287703	450276	96980
FP	102322	292377	22910	155064
FN	316727	7282	115814	132850
TN	988583	1198964	1197326	1401432
IoU	**0.474707**	**0.489822**	**0.764475**	**0.251965**
IoU score		**49.5%**		

Epoch 6

	road	building	vegetation	Bare soil
Road	387370	13656	85240	2259
Building	29807	390118	143738	19552
Vegetation	7799	370	451889	126
Bare soil	99748	22125	83433	50507
Overall accuracy				**71.6%**

IoU computation table

	road	building	vegetation	bare soil
TP	387370	390118	451889	50507
FP	101155	193097	8295	205306
FN	137354	36151	312411	21937
TN	1161858	1168371	1015142	1509987
IoU	**0.618922**	**0.629867**	**0.584898**	**0.181843**
IoU score		**50.4%**		

Epoch 7

	Road	Building	Vegetation	Bare soil
Road	378794	6391	53334	53522
Building	68018	384302	79427	59424
Vegetation	5810	283	445658	4669
Bare soil	46070	7053	22881	172101
Overall accuarcy				**77.2%**

IoU computation table

	road	building	vegetation	bare soil
TP	378794	384302	445658	172101
FP	113247	206869	10762	76004
FN	119898	13727	155642	117615
TN	1175798	1182839	1175675	1422017
IoU	**0.619006**	**0.635317**	**0.728126**	**0.470581**
IoU score		**61.3%**		

Epoch 8

	Road	Building	Vegetation	Bare soil
Road	486494	55554	45756	23527
Building	76891	369131	53465	2737
Vegetation	31357	5531	425017	1285
Bare soil	130429	32941	25899	20456
Overall accuracy				**72.8%**

IoU computation table

	road	building	vegetation	bare soil
TP	486494	369131	425017	20456
FP	124837	133093	38173	189269
FN	238677	94026	125120	27549
TN	936462	1190220	1198160	1549196
IoU	**0.57234**	**0.619088**	**0.722437**	**0.086213**
IoU score		**50.0%**		

Appendix E: Ground truth for the class change detection

Epoch 2-epoch 1

Epoch 3-epoch 2

Epoch 4-epoch 3

Epoch 6-epoch 5

Epoch 7-epoch 6

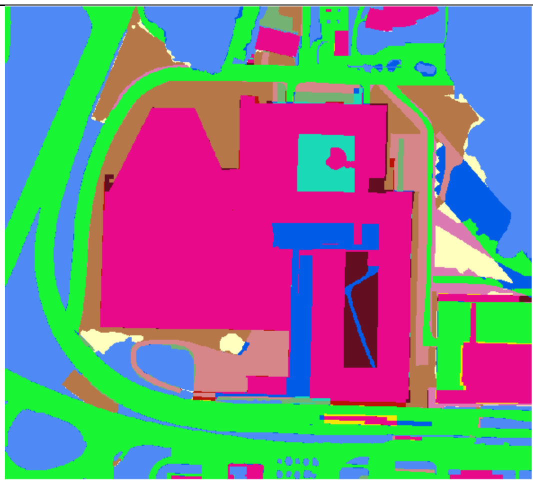

Epoch 8-epoch 7

Appendix F: Confusion matrix for post classification change detection

Epoch 6 –epoch 5 confusion matrix

Reference / Predicted	bs-rd	veg-rd	bld-rd	rd	bs-bld	veg-bld	bld	rd-bld	bs-veg	veg	bld-veg	rd-veg	bs	veg-bs	bld-bs	rd-bs
bs-rd	91	296	3	2723	27	1	24	226	550	660	2	422	3	0	0	0
veg-rd	1177	1571	0	804	11	20	4	2	142	1256	7	1433	3	9	0	1
bld-rd	2	0	0	201	6	0	122	34	85	1	3	1786	0	0	0	0
rd	43821	6067	512	324375	4273	380	2678	5398	9426	26954	789	47115	958	43	1	1221
bs-bld	24	0	10	478	3010	20	192	1409	769	1	51	1413	4849	21	11	15
veg-bld	0	5	0	13	53	187	3	2	48	209	7	8	0	2	0	0
bld	3139	6232	4068	14997	24357	47734	218809	78861	30816	24030	23109	76441	8209	481	7278	890
rd-bld	15	0	31	220	4	0	63	201	15	4	7	104	0	0	0	0
bs-veg	49	57	2	100	0	18	83	7	614	1426	109	641	5	3	0	0
veg	575	2472	8	3566	0	13	47	124	3365	436113	315	7260	3	65	0	3
bld-veg	2	75	0	36	0	6	26	28	12	88	19	86	11	0	0	9
rd-veg	135	123	1	420	1	7	7	0	360	639	13	811	3	2	0	0
bs	19649	781	437	67368	6208	301	442	10254	10902	7348	658	56474	50342	80	59	326
veg-bs	2630	5015	1	89	52	41	4	1	493	3077	0	716	121	40	0	0
bld-bs	68	43	64	3378	107	48	146	1326	0	302	445	1962	101	1	0	0
rd-bs	667	15	6	1638	109	0	10	70	66	150	3	904	62	13	0	106
													Overall accuracy			58.0%

IoU computation table

	bs-rd	veg-rd	bld-rd	rd	bs-bld	veg-bld	bld	rd-bld	bs-veg	veg	bld-veg	rd-veg	bs	veg-bs	bld-bs	rd-bs
TP	91	1571	0	324375	3010	187	218809	201	614	436113	19	811	50342	40	0	106
FP	4937	4869	2240	149636	9263	350	350642	463	2500	17816	379	1711	181287	12240	7991	3713
FN	71953	21181	5143	96031	35208	48589	3851	97742	57049	66145	25518	196765	14328	720	7349	2465
IoU	0.001182	0.056877	0	0.569037	0.063394	0.003807	0.381664	0.002043	0.010206	0.83856	0.000733	0.00407	0.204678	0.003077	0	0.016868
				IoU score			13.5%									

Epoch7-epoch6 confusion matrix

Reference / Predicted	bs-rd	veg-rd	bld-rd	rd	bs-bld	veg-bld	bld	rd-bld	bs-veg	veg	bld-veg	rd-veg	bs	veg-bs	bld-bs	rd-bs
bs-rd	5	117	9	396	0	0	0	2	13	917	2	108	0	883	100	458
veg-rd	0	680	1	636	0	0	0	0	0	5679	13	182	4	3195	17	107
bld-rd	0	26	27	218	0	0	58	1	0	68	3	114	0	94	166	123
rd	57	36758	4152	345101	5	165	5179	924	127	33978	1130	9564	1853	14492	2583	21551
bs-bld	3	9990	67	1209	2	87	128	3700	128	752	20	6	6517	1072	168	339
veg-bld	0	123	36	130	0	63	63	0	0	186	20	3	18	165	33	9
bld	190	25861	12168	19557	5789	60210	289772	5091	779	42234	36123	440	9711	26599	28456	2712
rd-bld	0	90	20	133	0	0	74	19	0	7	5	12	0	56	8	18
bs-veg	0	60	3	365	0	0	0	0	304	9199	50	1122	14	518	82	717
veg	0	921	8	2735	0	226	44	0	8	428563	16	2472	3	1848	0	679
bld-veg	0	2	26	71	0	7	6	0	0	181	60	31	0	0	0	0
rd-veg	0	738	7	1184	0	0	0	0	18	2880	6	645	39	208	27	327
bs	1099	7330	2512	44273	0	884	2807	1692	527	5655	1795	3515	42639	46091	11376	43986
veg-bs	0	1286	2	427	0	41	0	0	8	2628	3	18	63	6482	111	229
bld-bs	7	2	82	628	0	147	282	75	1126	430	3765	231	4154	1193	3978	141
rd-bs	24	612	17	1629	0	0	1	1	0	491	0	611	116	448	17	418
													Overall accuracy			62.6%

IoU computation table

	bs-rd	veg-rd	bld-rd	rd	bs-bld	veg-bld	bld	rd-bld	bs-veg	veg	bld-veg	rd-veg	bs	veg-bs	bld-bs	rd-bs
TP	5	680	27	345101	2	63	289772	19	304	428563	60	645	42639	6482	3978	418
FP	3005	9834	871	132518	24186	786	275920	423	12130	8960	324	5434	173542	4816	12263	3967
FN	1380	83916	19110	73591	5794	61767	8642	11486	2734	105285	42951	18429	22492	96862	43144	71396
IoU	0.001139	0.007201	0.001349	0.626079	6.67E-05	0.001006	0.504536	0.001593	0.020042	0.78953	0.001385	0.026318	0.17865	0.05993	0.066987	0.005516
				IoU score			14.3%									

Epoch8-epoch7 confusion matrix

Reference / Predicted	bs-rd	veg-rd	bld-rd	rd	bs-bld	veg-bld	bld	rd-bld	bs-veg	veg	bld-veg	rd-veg	bs	veg-bs	bld-bs	rd-bs
bs-rd	36150	1031	108	4995	10095	451	0	252	2365	142	7	26	17473	84	0	995
veg-rd	1484	25577	0	897	4	464	0	73	81	1313	0	202	14	36	0	0
bld-rd	16045	2067	1535	1756	5	103	3309	19	6138	9024	5666	999	270	2	6	1
rd	33287	35087	3989	325635	44	1414	481	34597	250	7110	9	11507	1136	201	0	5060
bs-bld	1247	175	55	549	2092	4	105	161	102	31	69	1	611	4	0	40
veg-bld	0	66	0	53	0	51	11	15	0	94	10	5	0	0	0	0
bld	15896	18376	10283	28859	31907	26338	272803	17978	718	21575	30187	1202	2042	707	12654	776
rd-bld	414	114	440	1258	0	117	957	1223	1	0	5	4	0	0	0	0
bs-veg	5725	1403	83	238	0	9	0	13	3258	825	37	3978	728	28	0	9
veg	829	14299	0	3752	0	4230	71	71	513	369315	191	754	123	2152	0	16
bld-veg	325	261	527	145	0	30	1197	133	285	1193	24158	17392	35	0	0	0
rd-veg	369	1554	1	1367	0	5	0	23	22	1067	1	462	1	42	0	23
bs	53393	5001	653	32412	5363	5829	4390	12518	9526	2987	423	3611	13314	1746	0	132
veg-bs	1055	15041	0	147	16	973	0	104	338	6567	0	28	5	5366	0	3
bld-bs	1107	567	1712	182	271	3	578	59	806	455	383	64	31	14	0	12
rd-bs	10069	4057	19	5758	1	872	432	1216	7	54	0	38	25	1	0	12
													Overall accuracy			60.5%

IoU computation table

	bs-rd	veg-rd	bld-rd	rd	bs-bld	veg-bld	bld	rd-bld	bs-veg	veg	bld-veg	rd-veg	bs	veg-bs	bld-bs	rd-bs
TP	36150	25577	1535	325635	2092	51	272803	1223	3258	369315	24158	462	13314	5366	0	12
FP	38024	4568	45410	134172	3154	254	219498	3310	13076	27001	21523	4475	137984	24277	6244	22549
FN	141245	99099	17870	82368	47706	40842	11531	67232	21152	52437	36988	39811	22494	5017	12660	7067
IoU	0.167812	0.197897	0.023683	0.600609	0.039507	0.001239	0.541456	0.017042	0.086912	0.822981	0.292226	0.010324	0.076609	0.154818	0	0.000405
				IoU score			19.0%									

Appendix G: Confusion Matrix for post classification change detection method after adding more samples

Epoch 6-epoch 5 confusion matrix

	bs-rd	veg-rd	bld-rd	rd	bs-bld	veg-bld	bld	rd-bld	bs-veg	veg	bld-veg	rd-veg	bs	veg-bs	bld-bs	rd-bs
bs-rd	92	313	3	2739	27	2	24	226	552	642	11	395	2	0	0	0
veg-rd	1176	1610	0	1339	11	21	4	3	159	1225	9	867	5	10	0	1
bld-rd	2	0	0	201	6	0	124	32	90	1	21	1763	0	0	0	0
rd	46016	7349	827	325190	4450	381	2922	5401	10224	25587	788	42635	1041	55	1	1144
bs-bld	37	0	10	326	3068	21	194	1559	770	1	51	1414	4781	21	19	1
veg-bld	2	9	0	13	53	188	4	2	48	202	6	8	0	2	0	0
bld	3163	6241	4499	15022	16082	45215	249796	73613	32916	17985	27101	63090	8205	448	5383	692
rd-bld	23	0	62	196	7	0	91	159	20	4	27	75	0	0	0	0
bs-veg	49	57	2	102	0	18	84	7	616	1434	107	630	5	3	0	0
veg	575	2512	8	3652	0	13	48	125	3503	436172	329	6903	6	80	0	3
bld-veg	4	84	0	36	0	6	46	8	12	87	44	53	9	0	0	9
rd-veg	134	129	2	445	1	7	7	0	357	631	13	785	5	5	0	1
bs	20231	786	440	64712	6313	468	449	12836	10779	7205	655	56665	49658	80	61	291
veg-bs	2670	5016	1	90	50	42	4	1	505	3134	0	632	95	40	0	0
bld-bs	68	51	63	3367	98	22	194	1386	0	295	432	1913	101	1	0	0
rd-bs	682	15	6	1509	109	0	10	143	70	151	3	941	97	13	0	70
													Overall accuracy			59.8%

IoU computation table

	bs-rd	veg-rd	bld-rd	rd	bs-bld	veg-bld	bld	rd-bld	bs-veg	veg	bld-veg	rd-veg	bs	veg-bs	bld-bs	rd-bs
TP	92	1610	0	325190	3068	188	249796	159	616	436172	44	785	49658	40	0	70
FP	4936	4830	2240	148821	9205	349	319655	505	2498	17757	354	1737	181971	12240	7991	3749
FN	74832	22562	5923	93749	27207	46216	4205	95342	60005	58584	29553	177984	14352	718	5464	2142
IoU	0.001152	0.055513	0	0.57276	0.07771	0.004021	0.435446	0.001656	0.009759	0.851046	0.001469	0.004349	0.201877	0.003077	0	0.011743
					IoU score		13.9%									

Epoch 7-epoch 6 confusion matrix

	bs-rd	veg-rd	bld-rd	rd	bs-bld	veg-bld	bld	rd-bld	bs-veg	veg	bld-veg	rd-veg	bs	veg-bs	bld-bs	rd-bs
bs-rd	5	107	10	329	0	0	0	2	14	925	2	100	0	896	104	516
veg-rd	0	439	0	511	0	0	0	0	2	5634	13	198	10	3447	18	242
bld-rd	0	24	23	208	0	0	58	1	0	63	3	119	0	99	169	131
rd	42	29527	3112	344457	6	169	5204	951	139	33886	1160	11076	1867	16599	3996	25428
bs-bld	3	9985	67	1162	2	77	145	3749	128	749	22	6	6511	1058	166	358
veg-bld	0	122	36	131	0	62	64	0	0	186	20	3	16	159	33	17
bld	196	23704	12681	19713	3860	57717	313608	4928	757	38611	38472	449	9526	21568	16660	3242
rd-bld	0	73	17	128	0	0	73	17	0	7	5	12	0	61	11	38
bs-veg	0	55	3	370	0	0	0	0	303	9273	50	1045	15	519	82	719
veg	0	713	8	2789	0	225	45	0	18	428519	16	2533	9	1967	0	681
bld-veg	0	2	26	71	0	7	6	0	0	183	59	30	0	0	0	0
rd-veg	0	215	7	1551	0	0	0	0	26	2830	7	766	39	280	27	331
bs	1094	2354	1854	37228	89	1142	3040	2111	531	6835	3664	2402	41812	49458	12916	49651
veg-bs	0	698	1	405	0	41	0	0	9	2790	3	27	62	6887	113	262
bld-bs	8	2	88	588	10	148	429	39	1135	488	3897	134	4060	1122	3939	154
rd-bs	24	118	16	1592	0	0	1	3	0	539	3	424	116	936	17	596
														Overall accuracy		63.9%

IoU computation table

	bs-rd	veg-rd	bld-rd	rd	bs-bld	veg-bld	bld	rd-bld	bs-veg	veg	bld-veg	rd-veg	bs	veg-bs	bld-bs	rd-bs
TP	5	439	23	344457	2	62	313608	17	303	428519	59	766	41812	6887	3939	596
FP	3005	10075	875	133162	24186	787	252084	425	12131	9004	325	5313	174369	4411	12302	3789
FN	1367	67699	17926	66776	3965	59526	9065	11784	2759	102999	47337	18558	22231	98169	34312	81770
IoU	0.001142	0.005613	0.001222	0.632734	7.1E-05	0.001027	0.545636	0.00139	0.019943	0.792787	0.001236	0.031091	0.175377	0.062914	0.077918	0.006918
					IoU score		14.7%									

Epoch 8- epoch 7 confusion matrix

	bs-rd	veg-rd	bld-rd	rd	bs-bld	veg-bld	bld	rd-bld	bs-veg	veg	bld-veg	rd-veg	bs	veg-bs	bld-bs	rd-bs
bs-rd	37889	1038	71	3484	11817	439	0	301	2390	146	7	21	15547	78	0	946
veg-rd	1576	25576	0	805	4	466	0	75	76	1339	0	178	14	36	0	0
bld-rd	15847	2038	1777	1740	2	80	3335	19	5686	8756	6397	1000	259	2	6	1
rd	38251	35041	4037	318118	595	1402	490	36514	388	8792	9	9757	1142	168	0	5103
bs-bld	1316	186	71	562	2105	6	117	147	102	27	70	1	514	4	0	18
veg-bld	0	66	0	53	0	47	11	2	0	98	10	18	0	0	0	0
bld	16176	18437	10567	27371	17776	25940	301853	18673	498	21344	30128	1229	585	447	1269	8
rd-bld	459	114	440	1212	0	117	957	1228	1	0	5	0	0	0	0	0
bs-veg	5730	1408	83	240	1	9	0	17	3270	837	38	3980	708	12	0	1
veg	839	14269	0	3736	0	3768	71	63	512	371709	191	714	116	314	0	14
bld-veg	329	261	528	145	0	30	1234	133	286	1054	24272	17377	32	0	0	0
rd-veg	371	1499	1	1345	3	11	0	23	23	1183	1	428	1	25	0	23
bs	56252	5074	1196	27915	10074	7270	4752	6538	11142	3685	648	1592	13244	1783	0	133
veg-bs	1169	15037	0	35	16	973	0	100	342	6595	0	3	5	5365	0	3
bld-bs	929	566	1815	181	207	15	749	59	785	455	372	70	27	2	0	12
rd-bs	12074	4026	19	3781	181	886	432	1024	7	59	0	34	26	1	0	11
														Overall accuracy		62.0%

IoU score computation table

	bs-rd	veg-rd	bld-rd	rd	bs-bld	veg-bld	bld	rd-bld	bs-veg	veg	bld-veg	rd-veg	bs	veg-bs	bld-bs	rd-bs
TP	37889	25576	1777	318118	2105	47	301853	1228	3270	371709	24272	428	13244	5365	0	11
FP	36285	4569	45168	141689	3141	258	190448	3305	13064	24607	21409	4509	138054	24278	6244	22550
FN	151318	99060	18828	72605	40676	41412	12148	63688	22238	54370	37876	35974	18976	2872	1275	6262
IoU	0.168028	0.197949	0.027017	0.597503	0.045839	0.001127	0.598382	0.018	0.084777	0.824763	0.290484	0.010462	0.077781	0.165001	0	0.000382
					IoU score		19.4%									

Appendix H: Confusion Matrix for pre classification change detection method

Epoch 6-epoch 5 confusion matrix

Reference / Predicted	bs-bld	veg-bld	bld	rd-bld	bs-veg	veg	bld-veg	rd-veg	bs	veg-bs	bld-bs	rd-bs	bs-rd	veg-rd	bld-rd	rd
bs-bld	30	0	2739	0	0	2695	0	0	0	0	0	0	0	0	0	6809
vag-bld	0	0	0	0	0	21	0	0	0	0	0	0	0	0	0	516
bld	0	0	0	0	0	0	0	0	0	0	0	0	0	0	0	0
rd-bld	0	0	0	0	0	174	0	0	0	0	0	0	0	0	0	490
bs-veg	55518	0	150455	0	0	103553	0	0	0	0	0	0	0	0	0	263039
veg	0	0	1	0	0	338190	0	0	0	0	0	0	0	0	0	115738
bld-veg	0	0	35	0	0	156	0	0	0	0	0	0	0	0	0	207
rd-veg	0	0	0	0	0	1585	0	0	0	0	0	0	0	0	0	937
bs	2589	0	10497	0	0	108002	0	0	0	0	0	0	0	0	0	110541
veg-bs	43	0	0	0	0	7435	0	0	0	0	0	0	0	0	0	4802
bld-bs	96	0	272	0	0	3463	0	0	0	0	0	0	0	0	0	4160
rd-bs	19	0	153	0	0	2465	0	0	0	0	0	0	0	0	0	1182
bs-rd	0	0	25	0	0	1705	0	0	0	0	0	0	0	0	0	3298
veg-rd	0	0	0	0	0	2178	0	0	0	0	0	0	0	0	0	4262
bld-rd	0	0	0	0	0	290	0	0	0	0	0	0	0	0	0	1950
rd	432	0	607	0	0	73533	0	0	0	0	0	0	0	0	0	399439
												Overall accuracy				41.3%

Epoch7-epoch6 confusion matrix

Reference / Predicted	bs-bld	veg-bld	bld	rd-bld	bs-veg	veg	bld-veg	rd-veg	bs	veg-bs	bld-bs	rd-bs	bs-rd	veg-rd	bld-rd	rd
bs-bld	3744	0	3157	0	0	3	0	0	4	0	0	0	0	0	0	17280
vag-bld	0	0	0	0	0	15	0	0	0	0	0	0	0	0	0	834
bld	0	0	0	0	0	0	0	0	0	0	0	0	0	0	0	0
rd-bld	0	0	0	0	0	0	0	0	0	0	0	0	0	0	0	442
bs-veg	148513	0	3623	0	0	4689	0	0	6059	0	0	0	0	0	0	415242
veg	0	0	0	0	0	388585	0	0	0	0	0	0	0	0	0	48938
bld-veg	0	0	0	0	0	219	0	0	0	0	0	0	0	0	0	165
rd-veg	0	0	0	0	0	1426	0	0	0	0	0	0	0	0	0	4653
bs	2373	0	5195	0	0	11759	0	0	0	0	0	0	0	0	0	196854
veg-bs	0	0	0	0	0	2486	0	0	0	0	0	0	0	0	0	8812
bld-bs	411	0	219	0	0	579	0	0	4	0	0	0	0	0	0	15028
rd-bs	0	0	0	0	0	163	0	0	0	0	0	0	0	0	0	4222
bs-rd	0	0	0	0	0	1130	0	0	0	0	0	0	0	0	0	1880
veg-rd	0	0	3	0	0	2649	0	0	0	0	0	0	0	0	0	7862
bld-rd	0	0	0	0	0	1	0	0	0	0	0	0	0	0	0	897
rd	431	0	143	0	0	38243	0	0	0	0	0	0	0	0	0	438802
													Overall accuracy			46.5%

Epoch8-epoch7 confusion matrix

Reference / Predicted	bs-bld	veg-bld	bld	rd-bld	bs-veg	veg	bld-veg	rd-veg	bs	veg-bs	bld-bs	rd-bs	bs-rd	veg-rd	bld-rd	rd
bs-bld	0	0	2795	0	0	33	0	0	656	0	0	0	0	0	0	1762
vag-bld	0	0	1	0	0	73	0	0	28	0	0	0	0	0	0	203
bld	0	0	0	0	0	0	0	0	0	0	0	0	0	0	0	0
rd-bld	0	0	3475	0	0	0	0	0	156	0	0	0	0	0	0	902
bs-veg	0	0	243894	0	0	37936	0	0	47813	0	0	0	0	0	0	178992
veg	0	0	2140	0	0	308882	0	0	16069	0	0	0	0	0	0	69225
bld-veg	0	0	1285	0	0	19843	0	0	417	0	0	0	0	0	0	24136
rd-veg	0	0	192	0	0	1044	0	0	736	0	0	0	0	0	0	2965
bs	2075	0	26749	0	0	14504	0	0	40010	0	0	0	0	0	0	67960
veg-bs	0	0	558	0	0	4510	0	0	450	0	0	0	0	0	0	24125
bld-bs	0	0	1337	0	0	6	0	0	2872	0	0	0	0	0	0	2029
rd-bs	0	0	2239	0	0	279	0	0	402	0	0	0	0	0	0	19641
bs-rd	0	0	17820	0	0	563	0	0	11296	0	0	0	0	0	0	44495
veg-rd	0	0	484	0	0	1286	0	0	366	0	0	0	0	0	0	28009
bld-rd	0	0	3512	0	0	2	0	0	16769	0	0	0	0	0	0	26662
rd	1473	0	29273	0	0	26410	0	0	42372	0	0	0	0	0	0	360279
													Overall accuracy			39.7%